



Moisture source identification for precipitation associated with tropical cyclone development over the Indian Ocean: a Lagrangian approach

Albenis Pérez-Alarcón^{1,2} · José C. Fernández-Alvarez^{1,2} · Rogert Sorí^{1,3} · Raquel Nieto¹ · Luis Gimeno¹

Received: 1 February 2022 / Accepted: 18 July 2022 / Published online: 29 August 2022
© The Author(s) 2022

Abstract

In this study, we investigated the moisture sources for precipitation through a Lagrangian approach during the genesis, intensification, and dissipation phases of all tropical cyclones (TCs) that occurred over the two hemispheric sub-basins of the Indian Ocean (IO) from 1980 to 2018. In the North IO (NIO), TCs formed and reached their maximum intensity on both sides of the Indian Peninsula, to the east in the Bay of Bengal (BoB), and to the west in the Arabian Sea (AS). The oceanic areas where TCs occurred were their main moisture sources for precipitation associated with TCs. Additionally, for TCs over the BoB, continental sources from the Ganges River basin and the South China Sea also played a notable role; for TCs over the AS, the Somali Low-Level jet (along the African coast in a northerly direction) also acted as an essential moisture transport. In the South IO (SIO), the western, central, and eastern basins were identified as the preferred areas for the genesis and development of TCs. During TC activity, the central IO and the Wharton and Perth basins mostly supplied atmospheric moisture. The Mascarene High circulation was the main moisture transport mechanism for the precipitation of TCs formed in the SIO basin. In both basins, during their intensification process, TCs gained more moisture (even more intensely when reaching the hurricane category) than during the genesis or dissipation stages. Additionally, the modulation during monsoonal seasons of the moisture contribution to the TCs was more noticeable over the NIO basin than for the SIO. Overall, the moisture uptake for precipitation from the sources for TCs occurred slightly faster in the NIO basin than in the SIO basin.

Keywords Moisture uptake · Tropical cyclones · Lagrangian approach · Indian Ocean

1 Introduction

Tropical cyclones (TCs) are essential elements of the hydrological cycle in tropical and subtropical regions (Dominguez and Magaña 2018). However, the combined effects of extreme winds, precipitation, and storm surges cause significant economic losses and human death, especially in coastal regions (Boruff 2009). Therefore, the forecasting of

TC intensity and trajectory to reduce the negative effects of these storms has been of special interest to the international scientific community.

TCs are formed over the tropical and subtropical waters of different cyclogenetic basins: North Atlantic, Central and East Pacific, North-Western and South Pacific Ocean, North Indian Ocean (NIO), and South Indian Ocean (SIO). The warm waters of the oceans provide the energy source for TCs, and their intensification is led by the enhanced latent and sensible heat fluxes due to the evaporation and heat transfer from the surface of the warm oceans, moistening the TC boundary layer (Williams 2016).

The role of moisture in TC development is crucial. Wang et al. (2016) demonstrated that latent heating associated with the condensation of water vapour is an important source of potential energy for TC intensification, and Gray (1968) showed that the relatively moist layers near the mid-troposphere are a necessary factor for their genesis. Early findings of Gray (1977) suggested that when mid-level

✉ Albenis Pérez-Alarcón
albenis.perez.alarcon@uvigo.es

¹ Centro de Investigación Mariña, Universidade de Vigo, Environmental Physics Laboratory (EPhysLab), Campus As Lagoas s/n, 32004 Ourense, Spain

² Departamento de Meteorología, Instituto Superior de Tecnologías y Ciencias Aplicadas, Universidad de La Habana, 10400 La Habana, Cuba

³ Instituto Dom Luiz, Faculdade de Ciências da Universidade de Lisboa, 1749-016 Campo Grande, Portugal

relative humidity over the ocean is less than 60%, cumulus convection does not typically occur, and when relative humidity is less than 40%, cyclonic development is not possible. The intensity of storms in sheared environments is enhanced (suppressed) if there is an increasing (reducing) mid-tropospheric relative humidity (Emanuel et al. 2004). Moreover, a moistened environment is considered one of the most important factors for forecasting the intensity of TCs (Wu et al. 2015). Therefore, globally, identifying where the atmospheric moisture comes from to the TCs during their different life stages is necessary to improve the predictive power of numerical TC prediction models and to improve the understanding of the global hydrological cycle.

The focus of this study was the analysis of TCs that formed over the Indian Ocean (IO), namely the northern and southern basins, the site of most of the world's deadliest cyclones (Longshore 2009; Samson et al. 2014), mostly due to flash flooding caused by storm surges and heavy rainfall (Needham et al. 2015; Bousquet et al. 2021; Wahiduzzaman 2021). Therefore, knowing precisely the origin of the humidity that generates precipitation in TCs is crucial.

In addition to the more or less common characteristics that can facilitate or inhibit the development or maintenance of TCs, the IO is affected by one of the most prominent climatic systems worldwide, the monsoon. In fact, it is affected by different monsoonal regimes, and they modulate the occurrence and frequency of TCs in the basin. For instance, during the summer monsoon season over the IO and South Asia, the cyclonic vorticity to the north of the strong cross-equatorial low-level jet stream is a dynamic force for the genesis of depressions and cyclones north of the Bay of Bengal (BoB) (Muni 2009). Nevertheless, according to Li et al. (2013) and Yuan et al. (2019), TCs formed over the NIO basin exhibit a bimodal seasonal distribution caused by unfavourable environmental conditions during the monsoon season. Thus, the monsoonal system phases and their seasonally associated fluxes throughout the areas of the IO can play an important role, including moisture availability, in TC activity over the basin.

Various methods and approaches have been developed to identify and follow the atmospheric moisture that reaches or leaves a specific region. Eulerian (van der Ent et al. 2014), Lagrangian (Stohl and James 2005; Sodemann et al. 2008; Sprenger and Wernli 2015) and analytical (Martínez and Domínguez 2014; Ordóñez et al. 2012) models, and physical water vapour tracers using isotopes (Henderson-Sellers et al. 2002) are the most used (Gimeno et al. 2010, 2012, 2020). Lagrangian models are commonly used to study the water vapour budget of air parcels as they travel either forward or backward in time and space (Stohl and James 2005; Gimeno et al. 2010, 2012, 2020). Nevertheless, the moisture sources that supply the atmospheric humidity that generates TC precipitation during their genesis and intensification stages remain poorly studied in any basin. Using the Lagrangian FLEXible

PARTicle (FLEXPART) dispersion model (Stohl et al. 2005), Xu et al. (2017) investigated in the Pacific basin the physical processes that caused extreme precipitation in Japan during the landfall of Typhoon Fitow in 2013, and Pazos and Gimeno (2017) studied over the North Atlantic Ocean the climatological moisture sources during the genesis phase of 110 TCs formed in the eastern part of the basin; Pérez-Alarcón et al. (2021) extended the study to the whole basin and to further phases of TC development.

In this study, we aim to investigate the origin of the moisture that becomes in precipitation associated with TCs formed over the IO by using a Lagrangian approach. The analysis also attempts to show the differences by considering the different regions of occurrence for the three life phases of the TCs: during their genesis, lifetime maximum intensity (LMI), and dissipation.

1.1 Study area

The IO is an ocean surrounded by large landmasses at low latitudes and the Indonesian archipelago (Fig. 1), which favours the formation of the monsoon system and the reversal of ocean currents. According to Hermes et al. (2019), the IO's climate is unique. The sea surface temperature (SST) at low latitudes is commonly characterised by values higher than 28 °C, which leads to the maintenance of atmospheric deep convection and seasonal air–sea interactions (DeMott et al. 2015).

The atmospheric transport patterns over the northern IO are mainly modulated by the seasonally reversing monsoon winds (Tegtmeier et al. 2022) and the Somali Low-Level Jet (SLLJ) positioned on the northeastern African continent. This configuration is crucial for moisture and momentum transport in regional circulation towards the Indian Peninsula (IP) (Halpern and Woiceshyn 1999; Viswanadhapalli et al. 2020). Over the southwest IO, the moisture fluxes and the low-level convergence of circulations associated with the Angola thermal low (ATL, positioned over the Angola–Namibia border), the Mascarene High pressure system (MHPS, Manatsa et al. 2014) positioned over 25–35° S and 40–110° E, and the flow from the northeast monsoon region through the tropical IO results in the formation of the SIO Convergence Zone (SICZ) during the austral summer (Ninomiya 2008; Lazenby et al. 2016; Barimalala et al. 2018). Furthermore, the northern branch of the MHPS plays an important role in defining the trajectories of TCs formed in the western SIO (Xulu et al. 2020).

2 Materials and methods

2.1 Data

We used the best track TC archive of the Joint Typhoon Warning Centre (JTWC), which provides complete data

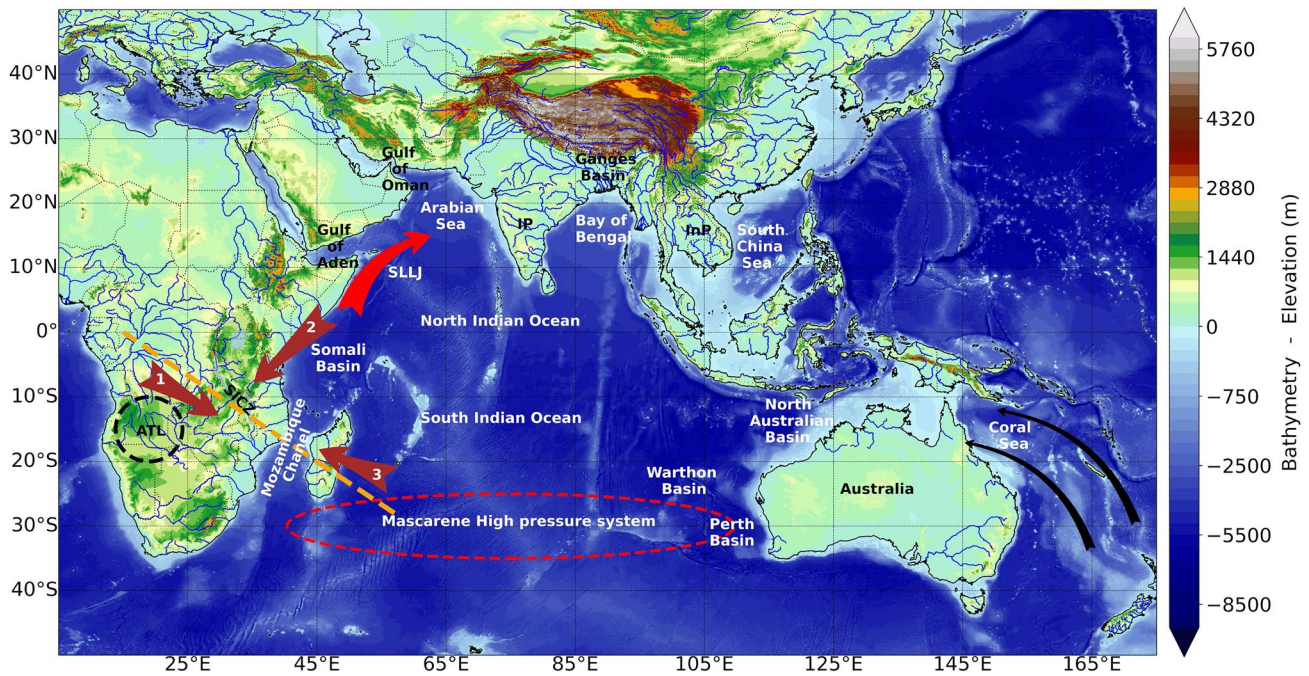


Fig. 1 Indian Ocean and surrounding landmasses. The red arrow represents the position of the Somali Low-Level Jet (SLLJ). The dashed orange line shows the mean location of the South Indian Ocean Convergence Zone (SICZ) during the austral summer. Brown arrows represent the major flows of moisture at low levels from: (1) the northern branch of the circulation of the Angola Thermal Low (ATL, black

dashed circle), (2) northeast monsoon region, (3) and northern branch of the Mascarene High pressure system (dashed red line). Black arrows represent the South-East trade winds at the east of Australia. IP denotes the Indian Peninsula, and InP denotes the Indochina Peninsula

on the systems formed over the NIO and SIO during their lifetime. The period available, from 1980 to 2018, is in the post-satellite era, for which TC records are considerably better than those in the pre-satellite era (Mohapatra et al. 2012). The best track dataset has a text format that contains the location, maximum winds, and minimum central pressure of all known tropical and subtropical cyclones every 6 h.

To compute the vertically integrated moisture flux (VIMF), we used the vertically integrated northward and eastward moisture flux every 6 h extracted from the European Centre for Medium-Range Weather Forecasts (ECMWF) ERA-Interim reanalysis (Dee et al. 2011). The ERA-Interim reanalysis is based on 4D-Var variational analysis in ECMWF's Integrated Forecast System from 1979 to 2019 with a spatial resolution of $1^\circ \times 1^\circ$ in latitude and longitude, and 61 vertical levels from the surface up to 0.1 hPa.

To determine the onset and offset of the monsoon system to investigate its relationship with variations in moisture sources during the phases of the TCs, we used daily precipitation data over the extended period of the study from the Multi-Source Weighted-Ensemble Precipitation (MSWEP) v2 dataset. This database incorporates a wide range of data from different sources (Beck et al. 2019).

2.2 Methodology

2.2.1 Cluster analysis

We objectively grouped TC genesis, lifetime maximum intensity (LMI), and dissipation locations in clusters using the K-means cluster technique (MacQueen 1967). The K-means algorithm divides N points in D dimensions into k clusters, where the addition of the variance within a cluster is minimised to ensure that the objects of each cluster are as close to each other as possible (Hartigan and Wong 1979). The optimal cluster number was determined by the maximum mean and minimum number of negative silhouette values. The silhouette value for each observation is a measure of the similarity of these observations within the same cluster when compared with observations in other clusters (Rousseeuw, 1987; Kaufman and Rousseeuw 2005). This clustering technique is one of the most used because of its simplicity, and it is used for clustering TCs in different basins (e.g. Nakamura et al. 2009; Corporal-Lodangco et al. 2014; Rahman et al. 2018; Pérez-Alarcón et al. 2022a).

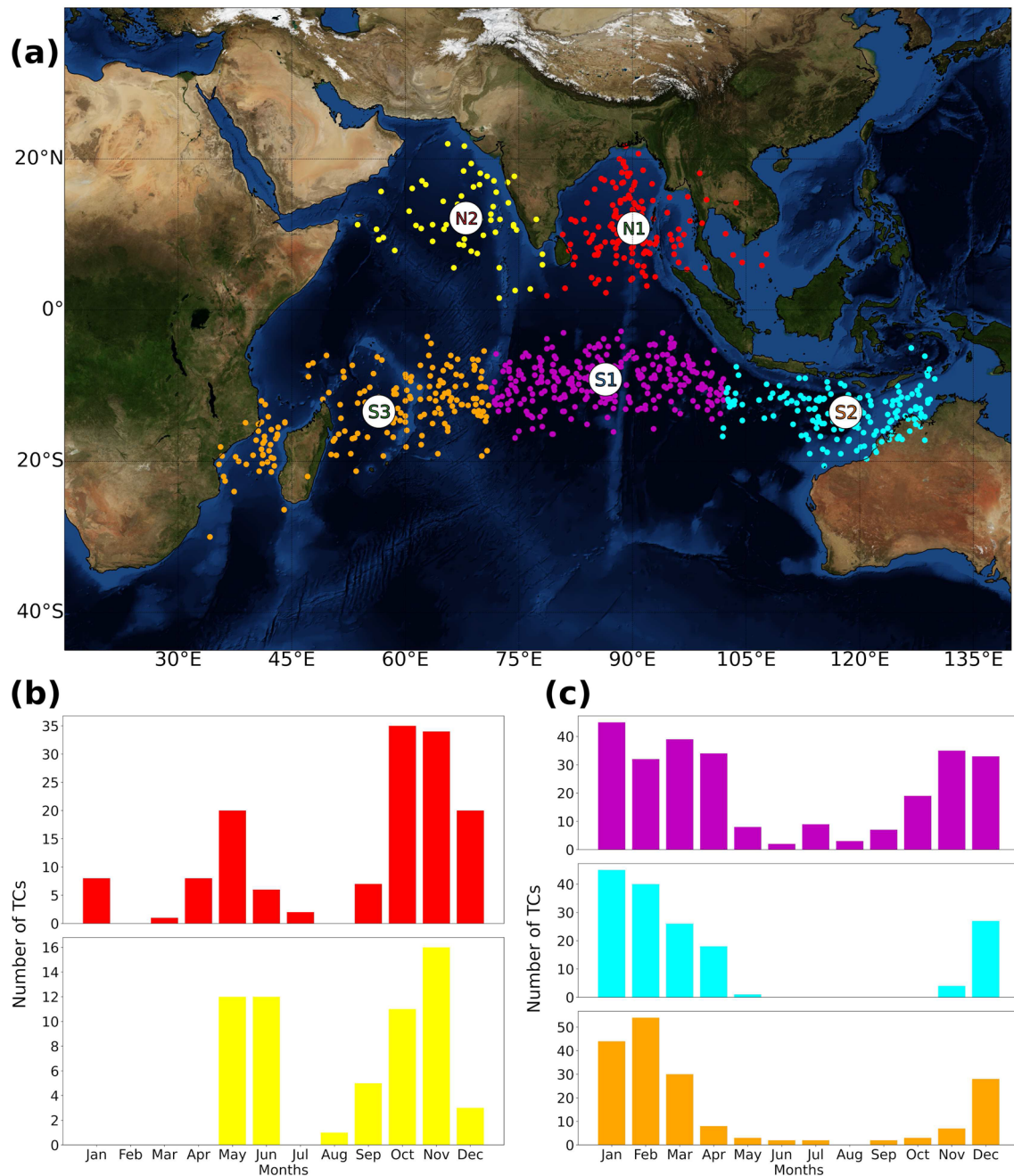


Fig. 2 **a** Genesis points of tropical cyclones (TCs) in the Indian Ocean from 1980 to 2018. Colours represent each cluster calculated by K-means for the North Indian Ocean (Nn, n=1, 2) and South

Indian Ocean (Sn, n=1, 2, 3). **b** Monthly frequency of TCs by cluster for the North Indian Ocean and **c** South Indian Ocean

2.2.2 Moisture sources diagnostic

To determine the origin of the precipitation that occurred during the genesis, the LMI, and the dissipation phases of TCs, we used the outputs from the Lagrangian model FLEXPART v9.0 (Stohl and James 2004, 2005). The model was forced using ERA-Interim reanalysis data (Dee et al. 2011) from the ECMWF at 6-h intervals with a 1° horizontal

resolution and 61 vertical levels covering the entire troposphere. FLEXPART was executed considering that the atmosphere was homogeneously divided into ~2.0 million parcels. It is worth noting that forcing the FLEXPART model with the ERA-5 reanalysis (Hersbach et al. 2020) at 0.25° horizontal resolution and 137 vertical levels or performing dynamic downscaling using the WRF (Skamarock et al. 2008) and FLEXPART-WRF (Brioude et al. 2013)

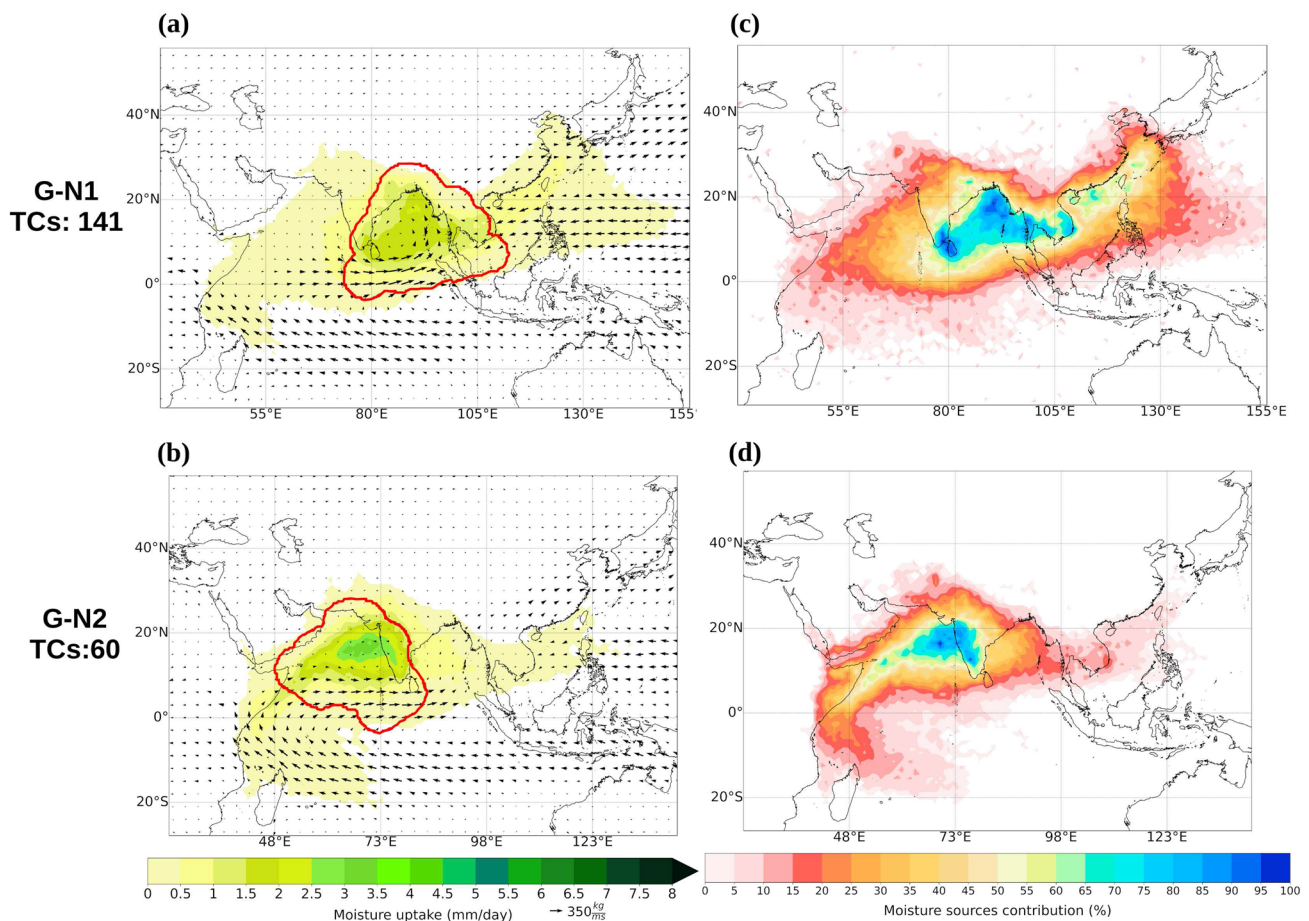


Fig. 3 **a, b** Composite of the moisture uptake (mm/day) pattern during the genesis phase of TCs and the vertically integrated moisture flux (VIMF) (arrows, kg/ms) for the North Indian Ocean. The red line

represents the area occupied by the size of all TCs (numbered on the left) within the cluster. **c, d** Composite of moisture sources contribution (%). Period of study: 1980–2018

models are not suitable for climatological long term studies due to the needed of high computing resources.

We focused on moisture sources for precipitation produced by TCs; thus, the trajectory of all precipitant parcels in the prior 6 h before arriving at the region of interest were followed backward in time up to 10 days. Several authors (Numaguti 1999; van der Ent and Tuinenburg 2017; Gimeno et al. 2021) have considered these 10 days as the average water vapour residence time in the atmosphere at a global scale. According to Läderach and Sodemann (2016), precipitant parcels were defined as those that achieved a decrease in specific humidity higher than 0.1 g/kg. Thus, for each parcel, the moisture variation ($e - p$) every 6 h was computed as

$$m \frac{dq}{dt} \approx m \left(\frac{\Delta q}{\Delta t} \right) = (e - p) \quad (1)$$

where e and p are the evaporation and precipitation from the environment, respectively, m is the mass of the parcel, and q is the specific humidity.

Therefore, by applying the methodology developed by Sodemann et al. (2008) for the identification of moisture sources, we identified regions where air masses gained moisture before the precipitation associated with each TC occurs and measured the moisture uptake (MU) during TC genesis, LMI, and dissipation phases. Further details of the moisture source diagnostic method are in Läderach and Sodemann (2016) and Pérez-Alarcón et al. (2022b). The region of interest around each TC, where the tracked atmospheric particles finally precipitated, was determined by the size of the TC. This target area was calculated as the region inside a circle delimited by the outer radius of the TC, which was computed as it was in Pérez-Alarcón et al. (2021, 2022c). After the individual MU for each TC was computed, a composite was performed to determine the total moisture uptake pattern for each genesis, LMI, and dissipation cluster.

Furthermore, a quantitative estimation of the moisture fractional contribution of each evaporative grid to the precipitation over the entire ocean basin was possible by using the moisture accounting method in Sodemann et al. (2008). The water

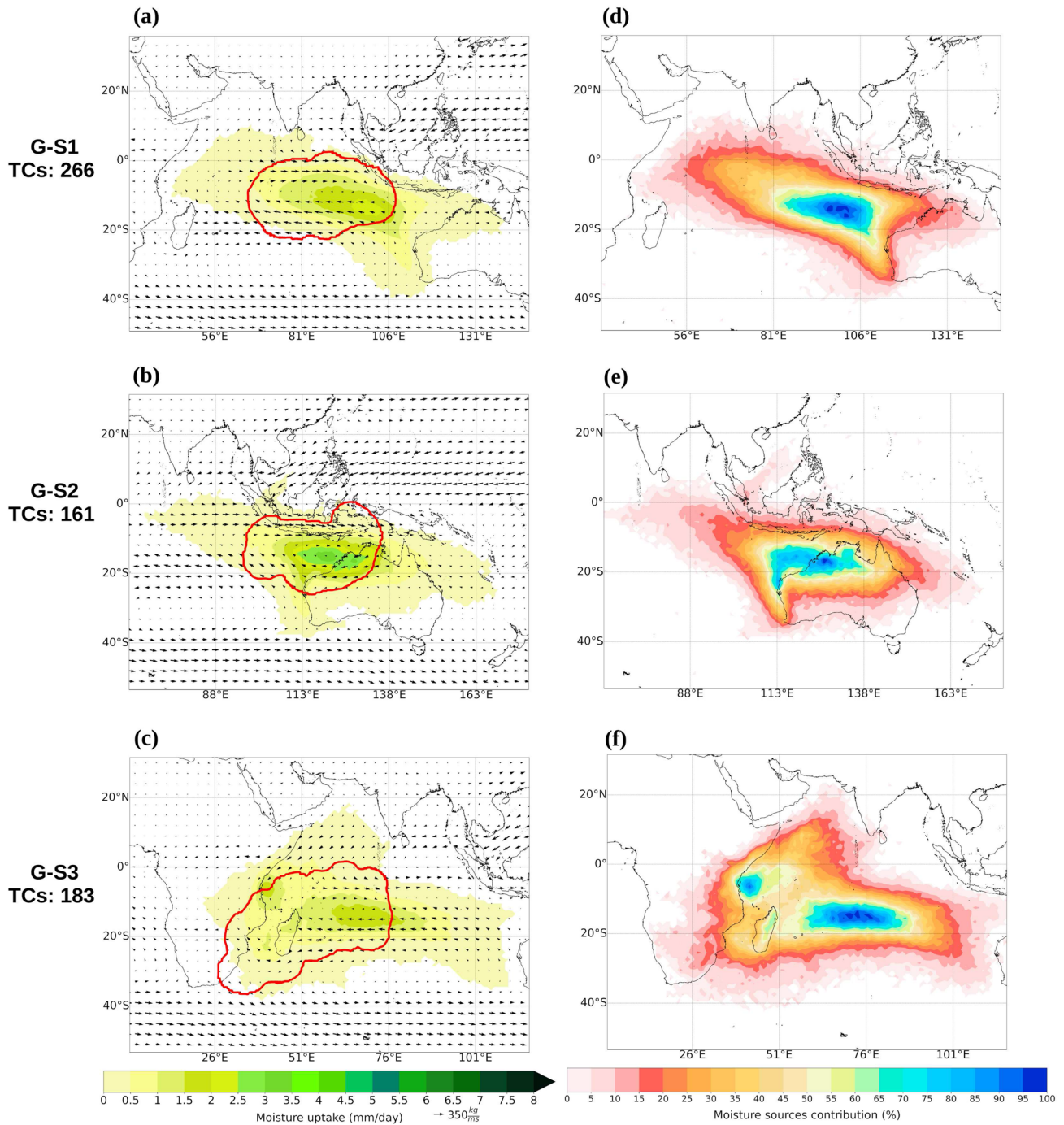


Fig. 4 **a–c** Composite of the moisture uptake (mm/day) pattern during the genesis phase of TCs and the vertically integrated moisture flux (VIMF) (arrows, kg/ms) for the South Indian Ocean. The red line

represents the area occupied by the size of all TCs (numbered on the left) within the cluster. **d–f** Composite of moisture sources contribution (%). Period of study: 1980–2018

vapour supplied by the moisture sources can be estimated by adding the individual fractional contributions over each grid cell. This methodology is similar to the Eulerian diagnostics of strong, large-scale ocean evaporation events (Aemisegger and Papritz 2018).

Moreover, the moisture source diagnostic method applied in this study permits an estimation of the time that an atmospheric parcel flows in the atmosphere before it precipitates, the known backward transit time, or water vapour residence time (WVRT) (Gimeno et al. 2021). The WVRT of each parcel

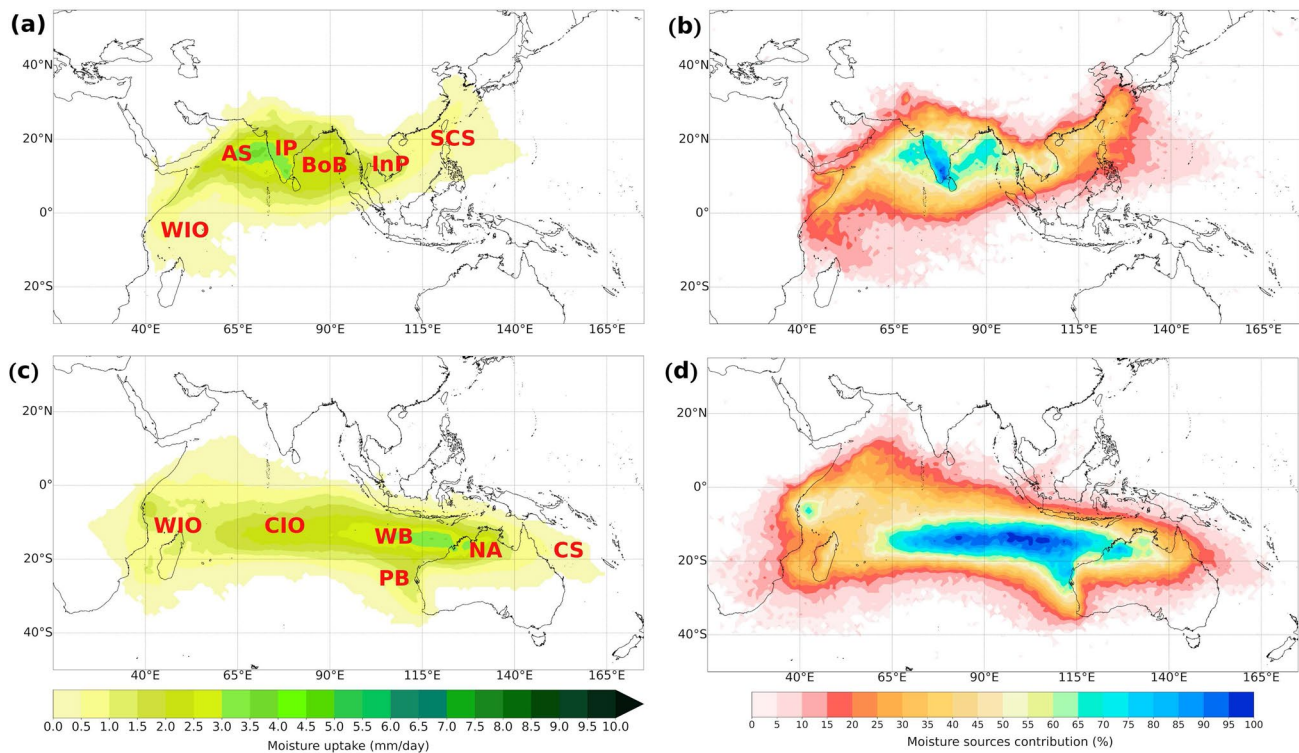


Fig. 5 Composite pattern of the moisture uptake (mm/day) for all TCs genesis locations for the **a** North Indian Ocean (NIO) and **c** South Indian Ocean (SIO); and moisture sources contribution composite for the **b** NIO and **d** SIO basins during the study period (1980–2018)

was estimated as the time between the far evaporation and precipitation within the TC limits, weighted by each evaporation location fractional contribution along the parcel trajectory. Therefore, by averaging the WVRT of all precipitant parcels over the target region, the Lagrangian mean residence time of water vapour (MWVRT) can be computed.

2.2.3 Determination of the monsoon onset and offset dates

To improve the understanding and elucidate the linkages between the monsoon systems and the extension and intensity of moisture sources for TC genesis, LMI, and the dissipation stages, we analysed the variability of moisture sources for the TCs during the pre-monsoon, monsoon, and post-monsoon phases.

To objectively determine the onset and offset dates throughout the year of the different monsoonal circulations over the study area (the Indian Summer Monsoon [ISM], the East Asian Summer monsoon [EASM], the Southeastern African Monsoon [SEAM], and the North Australia Monsoon [NAM]) we used the method in Noska and Misra (2016). This methodology was applied by Dunning et al. (2016) to study the onset and cessation of seasonal rainfall over Africa, and by Sorí et al. (2017) to investigate the atmospheric transport of moisture linked to monsoonal phases for the Indus, Ganges,

and Brahmaputra River basins. The methodology is based on computing the daily cumulative anomalies (C_m) of the average precipitation for an affected region throughout the year. The daily cumulative anomalies for day i of year m are computed as:

$$C'_m(i) = \sum_{n=1}^i [D_m(n) - R_c] \quad (2)$$

where $D_m(n)$ is the daily rainfall for day n of year m , and R_c is the climatology of the annual mean of the precipitation for N days ($N = 365$ or 366) for M years:

$$R_c = \frac{1}{MN} \sum_{m=1}^M \sum_{n=1}^N D(m, n) \quad (3)$$

The C'_m for the ISM, EASM, SEAM, and NAM were calculated over the limited regions defined as (7° – 22° N, 73° – 90° E), (5° – 45° N, 90° – 125° E), (0° – 40° S, 25° – 50° E) and (10° – 22° S, 110° – 140° E), respectively.

Therefore, the onset is defined as the day after the C'_m reaches its absolute minimum, and the offset is defined as the day when the C'_m reaches its absolute maximum after the onset date. We assumed the pre-monsoon from 60 days before the onset and the post-monsoon until 60 days after the offset, in agreement with Kiguchi and Matsumoto (2005).

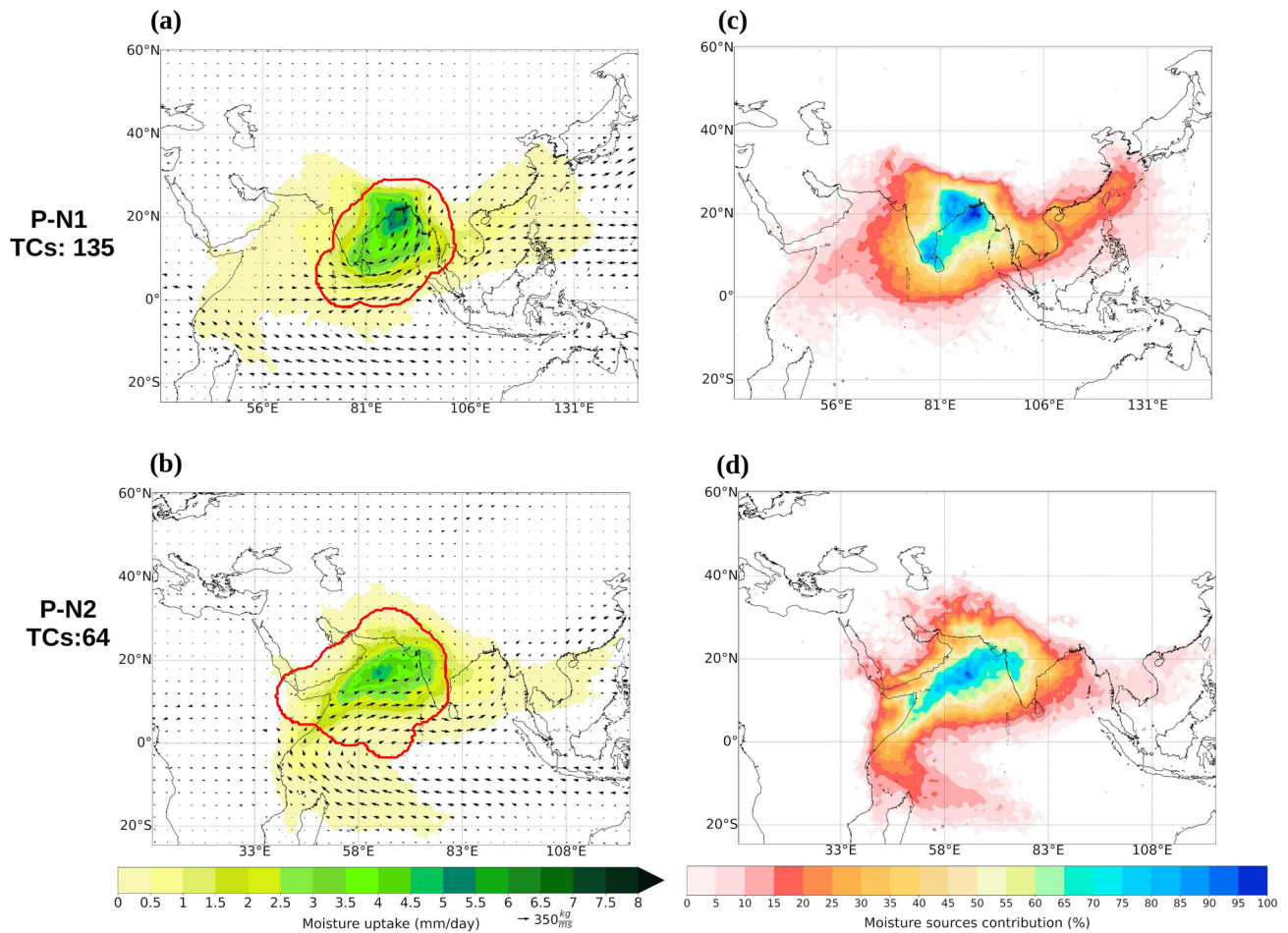


Fig. 7 **a, b** Composite of the moisture uptake (mm/day) pattern for the North Indian Ocean during TCs lifetime maximum intensity (LMI) phase and the vertically integrated moisture flux (VIMF)

(arrows, kg/ms). The red line represents the area occupied by the size of all TCs (numbered on the left) within the cluster. **c, d** Composite of moisture sources contribution (%). Period of study: 1980–2018

2012; Li et al. 2013). For the SIO basin, three regions of genesis were identified: the central tropical SIO (G-S1) with 43.6% of the events, northwest of Australia (G-S2, 26.4%), and the southwest IO (G-S3, 30%). Over the SIO basin, the highest TC frequency in each genesis cluster was observed in January and February (Fig. 2c), in agreement with Yuan et al. (2019).

The moisture uptake (MU) pattern over the NIO revealed that for the G-N1 region (Fig. 3a), the Bay of Bengal (BoB) was its main moisture source, contributing between ~50% and 70% of the atmospheric humidity (Fig. 3c), and the South China Sea (SCS) with a notable ~30–45%, and the Indian Peninsula (IP) with ~15–20%. The air masses reaching G-N2 gained moisture (Fig. 3b) mainly from the Arabian Sea (AS) and the southwestern portion of the IP, with a ~55–70% contribution (Fig. 3d), and the moisture contribution was lower from the SIO through the Somali Low-Level Jet (SLLJ) area of influence (~10–20%) and from the east African coast (~15–30%).

Over the SIO, the easterly trade winds blowing from the Mascarene High pressure system (MHPS) were the mainly mechanism of moisture transport from the Perth Basin (PB) and Wharton Basin (WB) to the G-S1 genesis cluster (Fig. 4a). The moisture contribution (Fig. 4d) from the WB ranged from 75 to 85%, and the PB supplied ~30–50%. For G-S2 (Fig. 4b, e), located over the North Australian Basin, the main moisture source was its region, supporting ~50–70%. The South-East trade winds transported moisture from the western Coral Sea (CS; ~10–25%), crossing north of Australia (Nieto et al. 2014). Additionally, the westerly winds linked to the Australian monsoon system during the warmer months in the South Hemisphere (Drosowsky 1996; Lisonbee et al. 2020) transported moisture (~5–25%) from the eastern tropical IO. Overall, these moisture transport patterns were supported by the VIMF field (Fig. 4b). For G-S3 (Fig. 4c, f), the MHPS also transported the majority of the atmospheric humidity (~65–90%) from the central

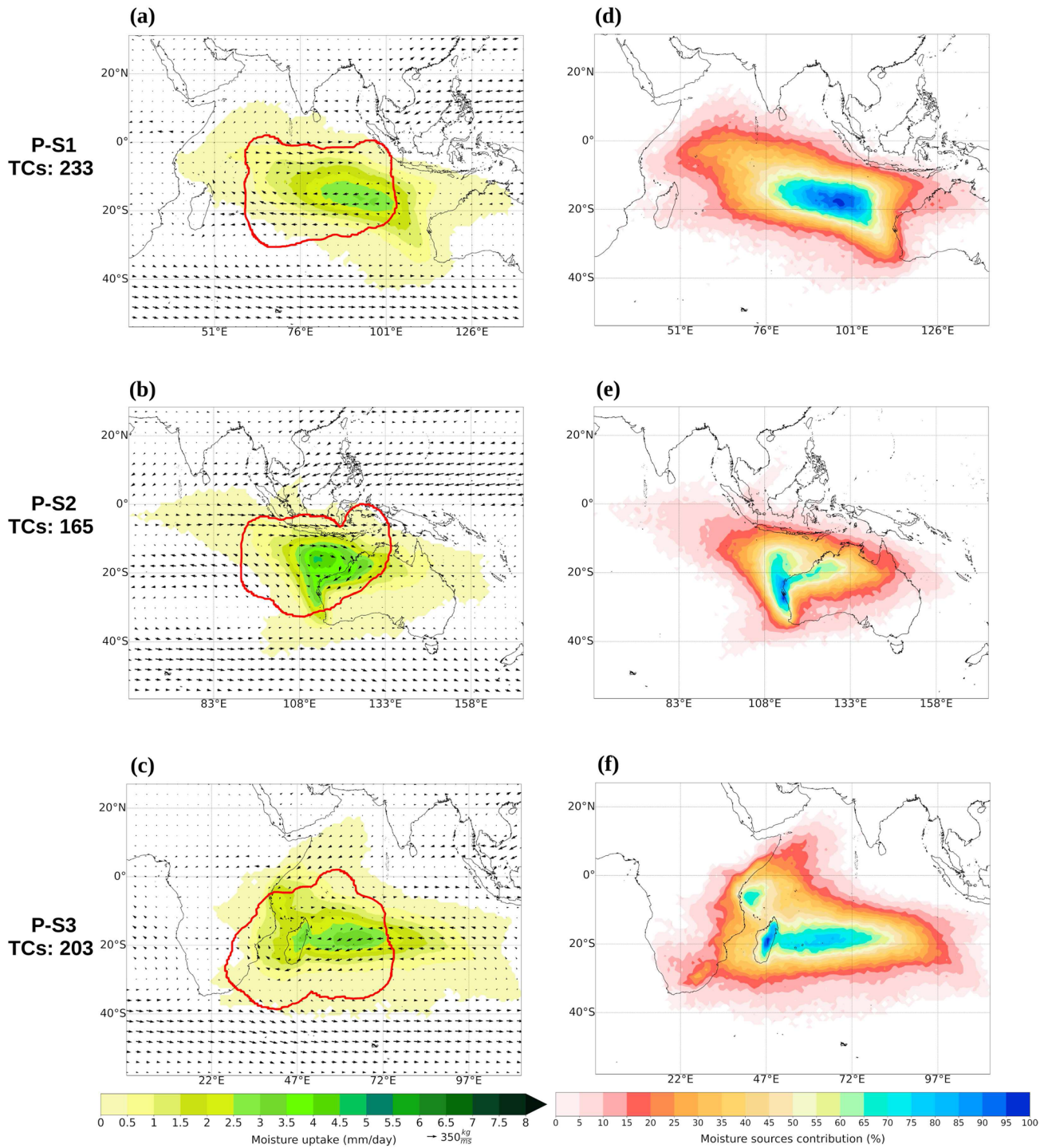


Fig. 8 a–c Composite of the moisture uptake (mm/day) pattern for the South Indian Ocean during TCs lifetime maximum intensity (LMI) phase and the vertically integrated moisture flux (VIMF)

(arrows, kg/ms). The red line represents the area occupied by the size of all TCs (numbered on the left) within the cluster. **d–f** Composite of moisture sources contribution (%). Period of study: 1980–2018

IO (CIO), and a secondary nucleus appeared over the Somali basin, exhibiting a moisture contribution of ~65%.

Several source regions contribute to moisture in various genesis areas; therefore, we analysed the total contribution

of moisture from each source to the cyclogenesis over both sub-basins. The total MU pattern of the precipitant parcels residing over the TC genesis regions over the IO is plotted in Fig. 5. The advection of oceanic moisture from the IO

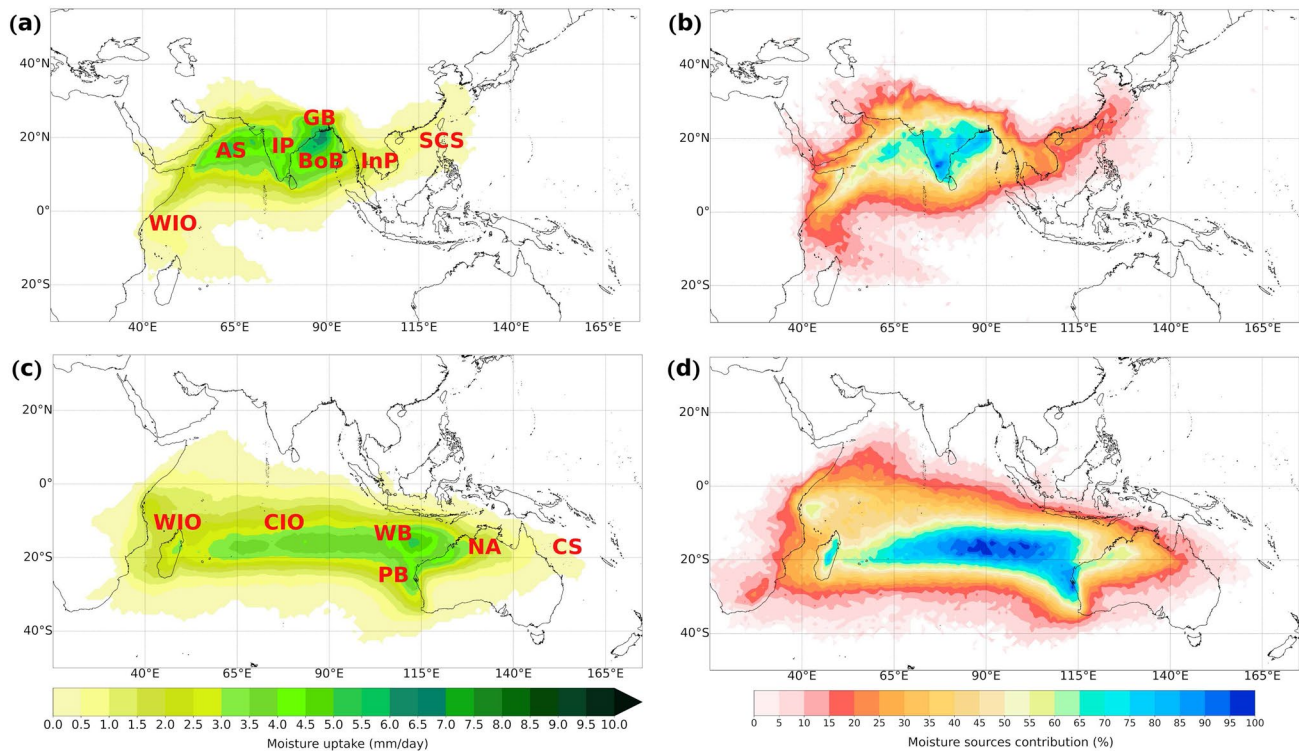


Fig. 9 The same as Fig. 5 but for the TCs lifetime maximum intensity

towards the TC genesis regions was higher than that from the subcontinental land. The oceanic and terrestrial sources in NIO contributed ~85.93% and ~14.07% of moisture, respectively, while the contributions from ocean and land regions accounted for ~80.29% and 19.71% in SIO, respectively. In summary, the results allowed the identification of six sources of moisture for cyclogenesis in the NIO basin (Fig. 5a): the Arabian Sea (AS), the Bay of Bengal (BoB), terrestrial moisture sources in the Indian (IP) and Indochina Peninsula (InP), the South China Sea (SCS), and the western IO (WIO) along the SLLJ jet. Overall, the IP, AS, and BoB contributed to the majority of the moisture (~70%), the moisture contributions from InP and SCS ranged from 20 to 30%, and the atmospheric humidity supported by the

WIO is less than 20% (Fig. 5b). Likewise, in the SIO basin (Fig. 5c), the moisture sources that supplied the atmospheric humidity during the genesis of TCs were the western IO (WIO), the central IO (CIO), the Wharton Basin (WB), the Perth Basin (PB), the Coral Sea (CS), and northern Australia (NA). As shown in Fig. 5d, the highest moisture contribution (~50–80%) was from CIO and WB, followed by NA (~40%) and WIO (~30%). Notably, the WIO exhibits nuclei with a maximum contribution of 60% over the Somali basin. Moreover, the moisture contribution from the CS was less than 10%.

From the different sources, the moisture lasted different times to become precipitation. The MWVRT for the whole sources over the NIO basin, calculated from the Lagrangian approach, during TCs genesis phases was 3.1 ± 0.5 days (variability indicated by one standard deviation), 3.2 ± 0.4 days for the Bay of Bengal (G-N1) cluster, and 2.9 ± 0.5 days for the cluster over the Arabian Sea (G-N2). For the whole SIO basin, the estimated MWVRT was higher than that in the NIO, at 3.3 ± 0.5 days. The central tropical SIO (G-S1) exhibited the highest values, 3.4 ± 0.5 days, followed by the western SIO (G-S3) and northeast Australia (G-S2), which showed 3.3 ± 0.5 days and 3.1 ± 0.5 days, respectively.

Table 1 Lagrangian mean water vapour residence time (MWVRT, in days) during the TCs lifetime maximum intensity (LMI), and for the TCs categorised by intensity: Tropical Storm (TS), Hurricanes (H, category 1 and 2 on the Saffir-Simpson scale), and Major Hurricane (MH, category 3+ on the Saffir-Simpson scale)

Basin	LMI	TS	H	MH
NIO	2.8 ± 0.5	3.0 ± 0.5	2.8 ± 0.5	2.7 ± 0.3
SIO	3.1 ± 0.5	3.2 ± 0.5	3.1 ± 0.4	3.1 ± 0.5

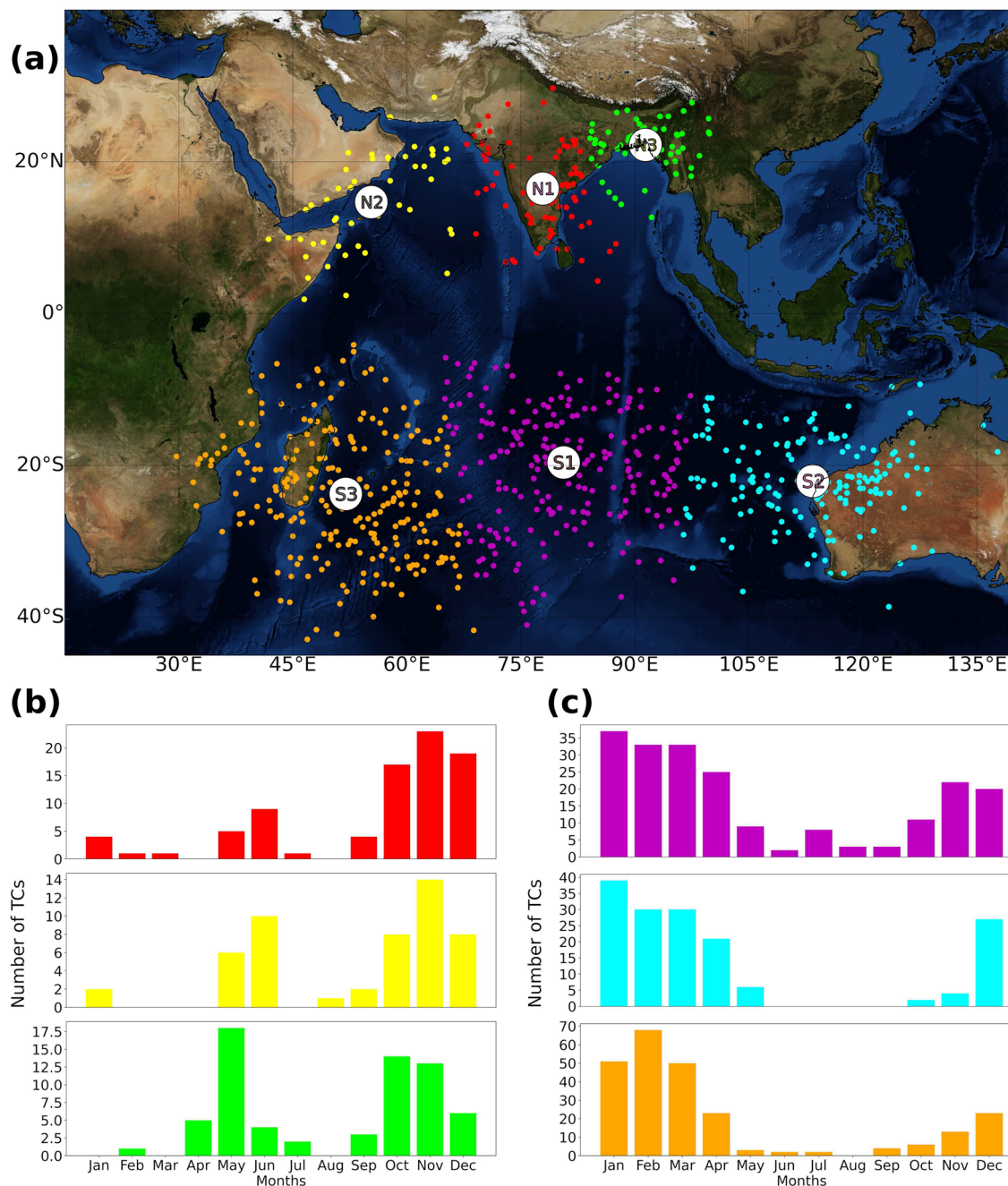


Fig. 10 a Dissipation points of tropical cyclones (TCs) formed over the Indian Ocean from 1980 to 2018. Colours represent each cluster calculated by K-means for the North Indian Ocean (Nn, $n=1, 2$)

and South Indian Ocean (Sn, $n=1, 2, 3$). The monthly frequency of TCs by cluster is also represented for the **b** North Indian Ocean and **c** South Indian Ocean

3.2 Origin of tropical cyclone precipitation in the lifetime maximum intensification phase

Cluster analysis (Fig. 6a) again revealed five regions in the IO basin where TCs reached the lifetime maximum intensity (LMI). For the NIO basin was the Bay of Bengal (P-N1) where 67.8% of the TCs showed their peak of intensification, and the Arabian Sea (P-N2) accounted the remaining 32.1%.

For the SIO basin was the central tropical South Indian Ocean (P-S1) where occurred 38.7% of the TCs during LMI, followed by the West Indian Ocean (P-S3, 33.7%), and the northwest of Australia (P-S2, 27.4%). For both basins, the monthly frequency showed a bimodal distribution, similar to that observed for genesis (Fig. 6b,c).

Figures 7a,b show that the evaporation of water over the BoB was the main region that supplied atmospheric

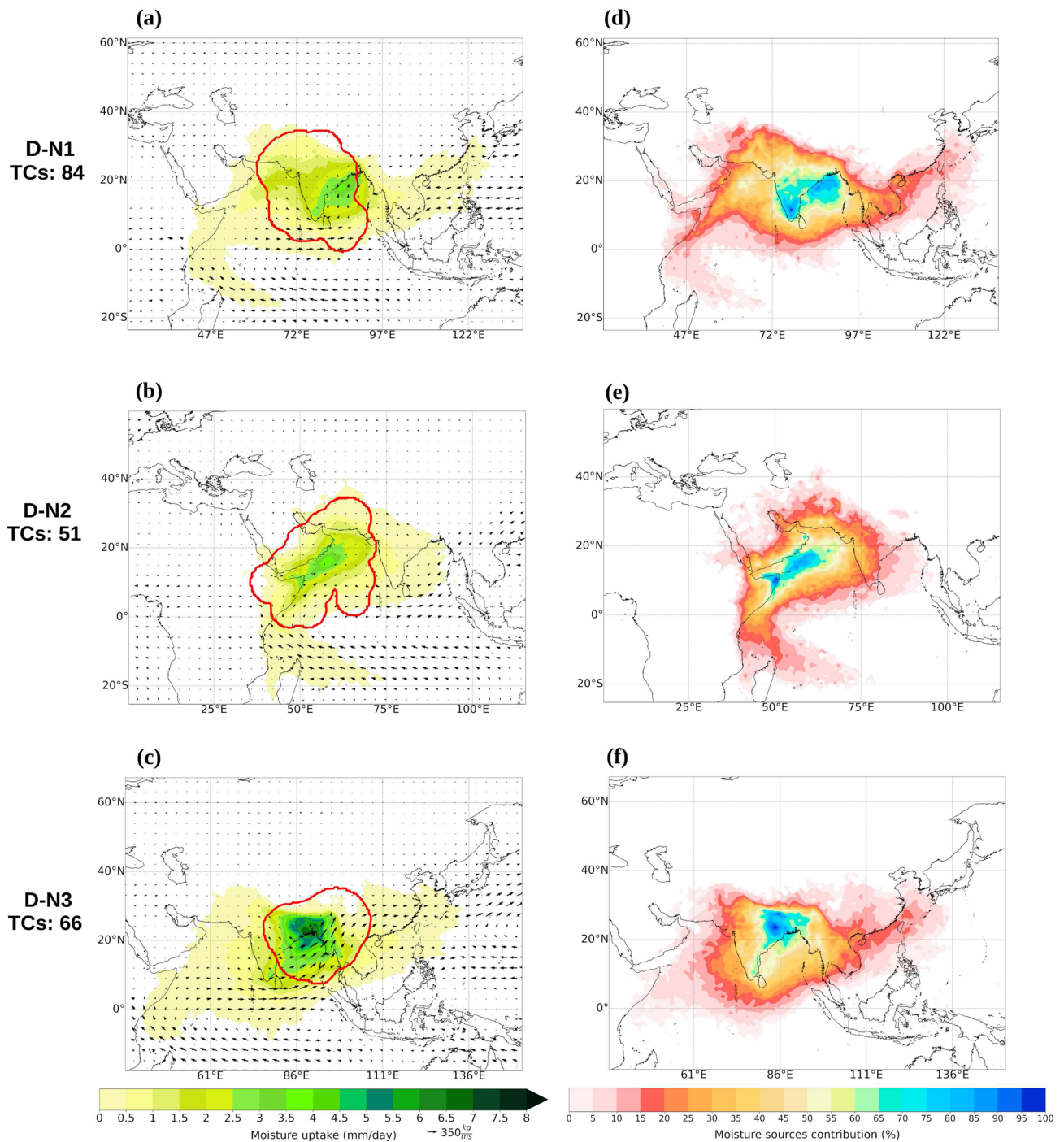


Fig. 11 a–c Composite of the moisture uptake (mm/day) pattern for the North Indian Ocean during the TCs dissipation phase and the vertically integrated moisture flux (VIMF) (arrows, kg/ms). The red line

represents the area occupied by the size of all TCs (numbered on the left) within the cluster. c–e Composite of moisture sources contribution (%). Period of study: 1980–2018

humidity (~60–75%) for the TCs in P-N1 during their LMI. In addition, P-N1 received, but in a smaller amount, moisture from the SCS (~25%), the IP (~15–25%), and from the AS (~5–10%), in Fig. 7b. The pattern changed for P-N2 (Fig. 7c), for which the AS supplied most of the moisture

(~60%), and not an inconsiderable amount arrives across the equator along the coast of East Africa and the Gulf of Aden (~25%) through the SLLJ (Fig. 7c), in agreement with Ordóñez et al. (2012).

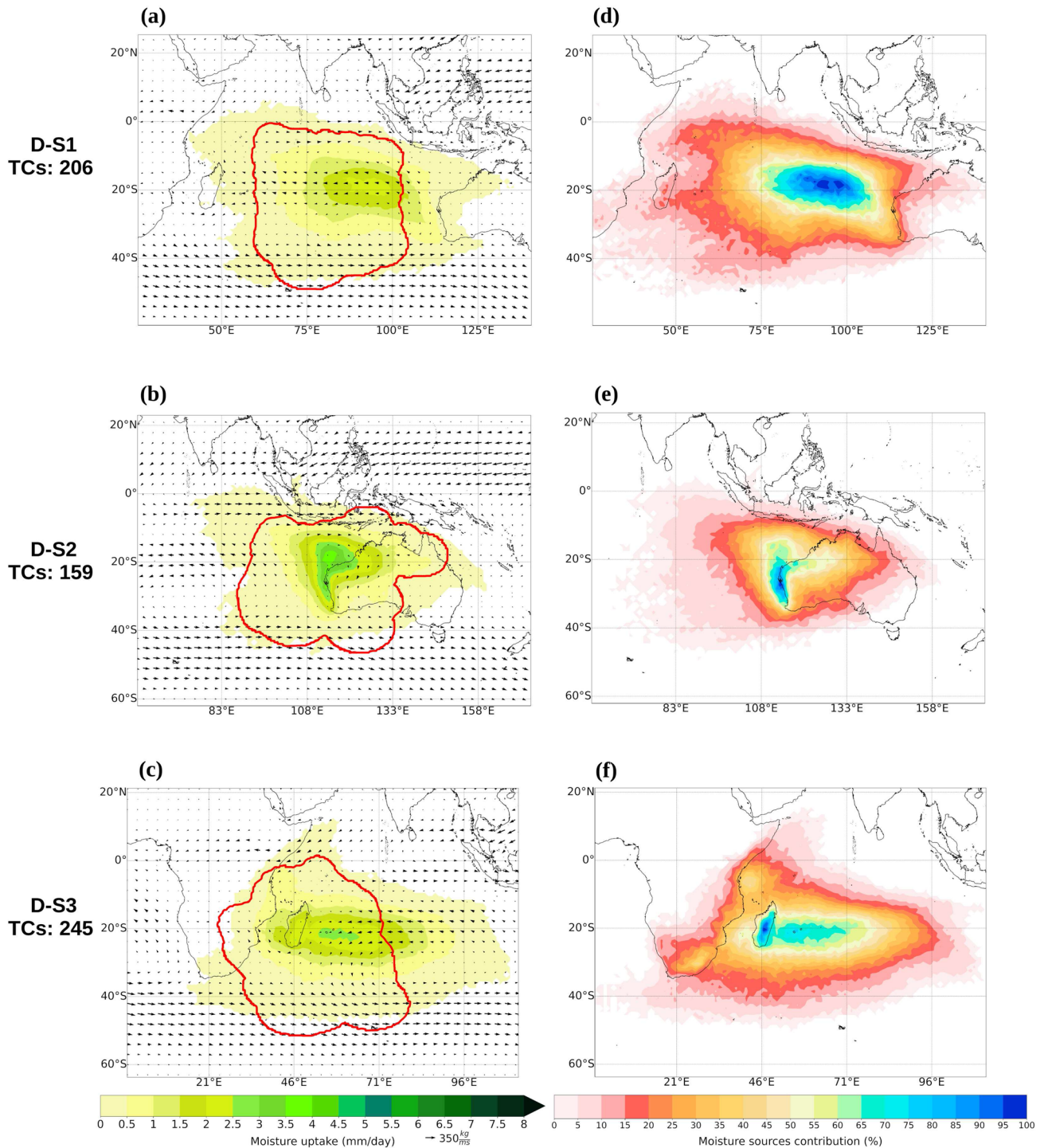


Fig. 12 a–c Composite of the moisture uptake (mm/day) pattern for the South Indian Ocean during the TCs dissipation phase and the vertically integrated moisture flux (VIMF) (arrows, kg/ms). The red line

represents the area occupied by the size of all TCs (numbered on the left) within the cluster. c–e Composite of moisture sources contribution (%). Period of study: 1980–2018

For the TC LMI phase over the SIO basin, the pattern of moisture uptake in each cluster was similar to that observed for TC genesis, but more intense (Fig. 8). The circulation pattern associated with the MHPS (see VIMF vectors,

Fig. 8a) transported moisture from the Wharton and Perth basins to P-S1 along its eastern branch, supplying approximately 50–70% of the moisture (Fig. 8d), and the northern branch towards the west supplied moisture from the central

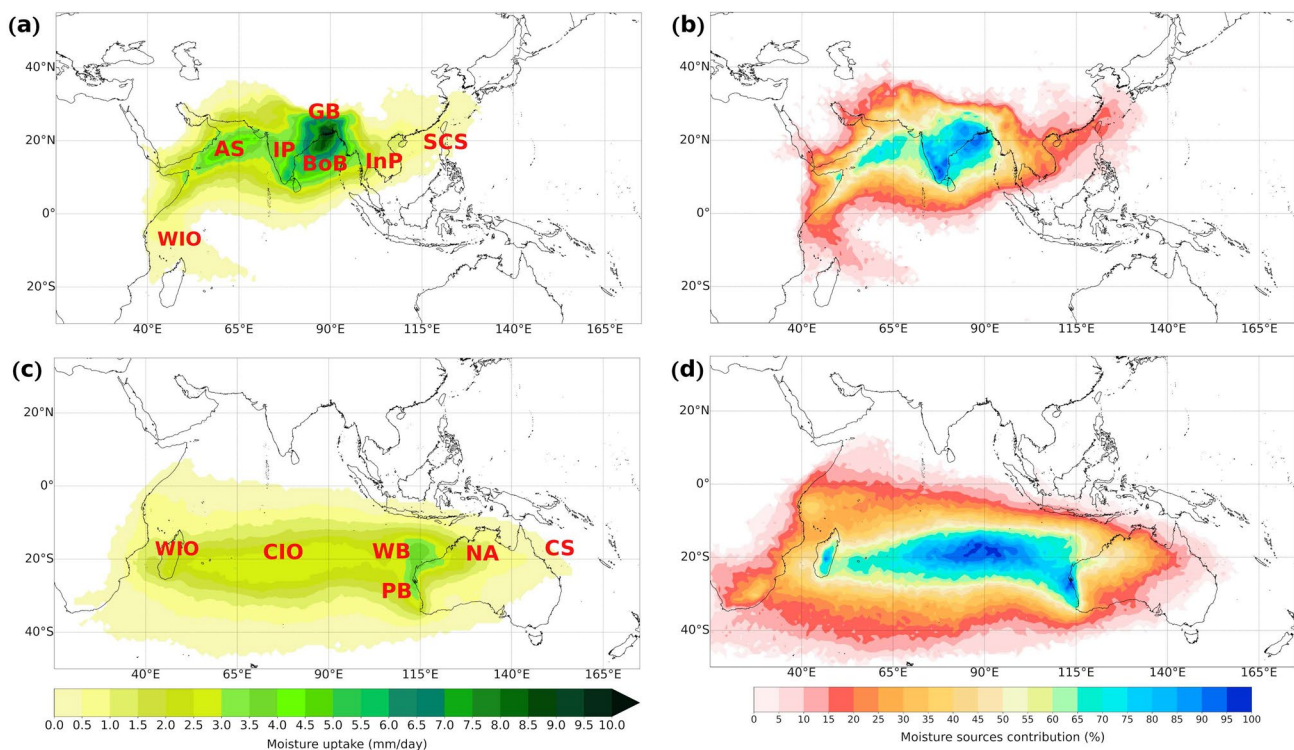


Fig. 13 The same as Fig. 5 but for the TCs dissipation phase

IO (~40–65%) to P-S3 (Fig. 8c, f). For P-S3, the flow from the northeast monsoon region from the northeastern coast of Africa and the Somali Basin also achieved ~20–40%. Furthermore, for P-S2 the importance of the moisture transported from inland northern Australia (~40–75%), and the winds related to the Australian monsoon, blowing from the northwest, also transported moisture (~5–25%) from the NOI towards P-S2 (Fig. 8b, e), complemented by the trade winds associated with high pressures around Australia from the Coral Sea (~5%), in agreement with Nieto et al. (2014).

Figure 9 summarises the moisture sources for the TCs during their LMI over the IO. Clearly, for the NIO basin, AS, BoB, Ganges basin (GB), and the IP were again the main moisture sources for this TC phase (Fig. 9a). The four supplied ~64% of the atmospheric humidity (Fig. 9b); the Indochina Peninsula (InP) and the South China Sea (SCS) provided ~27%; and the WIO, the remaining ~9%. Over the SIO basin (Fig. 9c), the unified area of the central IO, WB, and BP was the main moisture source for the TCs during the LMI phase, supplying most of the moisture (~63%), followed by the WIO (~22%) and northern Australia (NA) and western Coral Sea (CS) (~15%). Figure 9 also reveals that the moisture contributions from oceanic sources are notably higher than that from terrestrial sources during the LMI phase in both basins. Overall, the oceanic sources supplied ~84.33% (~78.19%) in the NIO (SIO) basin, while the terrestrial counterpart contributed ~15.67% (~21.81%).

The dynamic and thermodynamic processes leading to changes in TC intensity are a key factor in understanding TC development. Our findings revealed that intensity changes to hurricane category (NIO: 702.8 mm/day per TC, SIO: 765.1 mm/day per TC) required more atmospheric moisture than those to major hurricanes (NIO: 660.1 mm/day per TC, SIO: 705.4 mm/day per TC) or tropical storms (NIO: 575.8 mm/day per TC, SIO: 637.9 mm/day per TC) in the NIO and SIO basins. As a general feature, TCs during the LMI or intensity changes over the NIO gained less water vapour for precipitation than over the SIO. Additionally, like for LMI and genesis phases, the oceanic sources supplied the higher amount of moisture in both basins.

The MWVRT during TCs LMI and intensity changes (Table 1) was higher in the SIO (3.1 ± 0.5 days) than in the NIO (2.8 ± 0.5 days). On average, the moisture uptake that became precipitation during the tropical storm category (TS) exhibited higher MWVRT in both basins than during the hurricane category (H) and major hurricane category (MH).

3.3 Origin of tropical cyclone precipitation during the dissipation phase

The clusters for the TC dissipation phase over the NIO and SIO basins are shown in Fig. 10a. In this phase, three clusters appear in the NIO basin. The majority of TCs (41.7%) dissipated over the Indian Peninsula (D-N1, red),

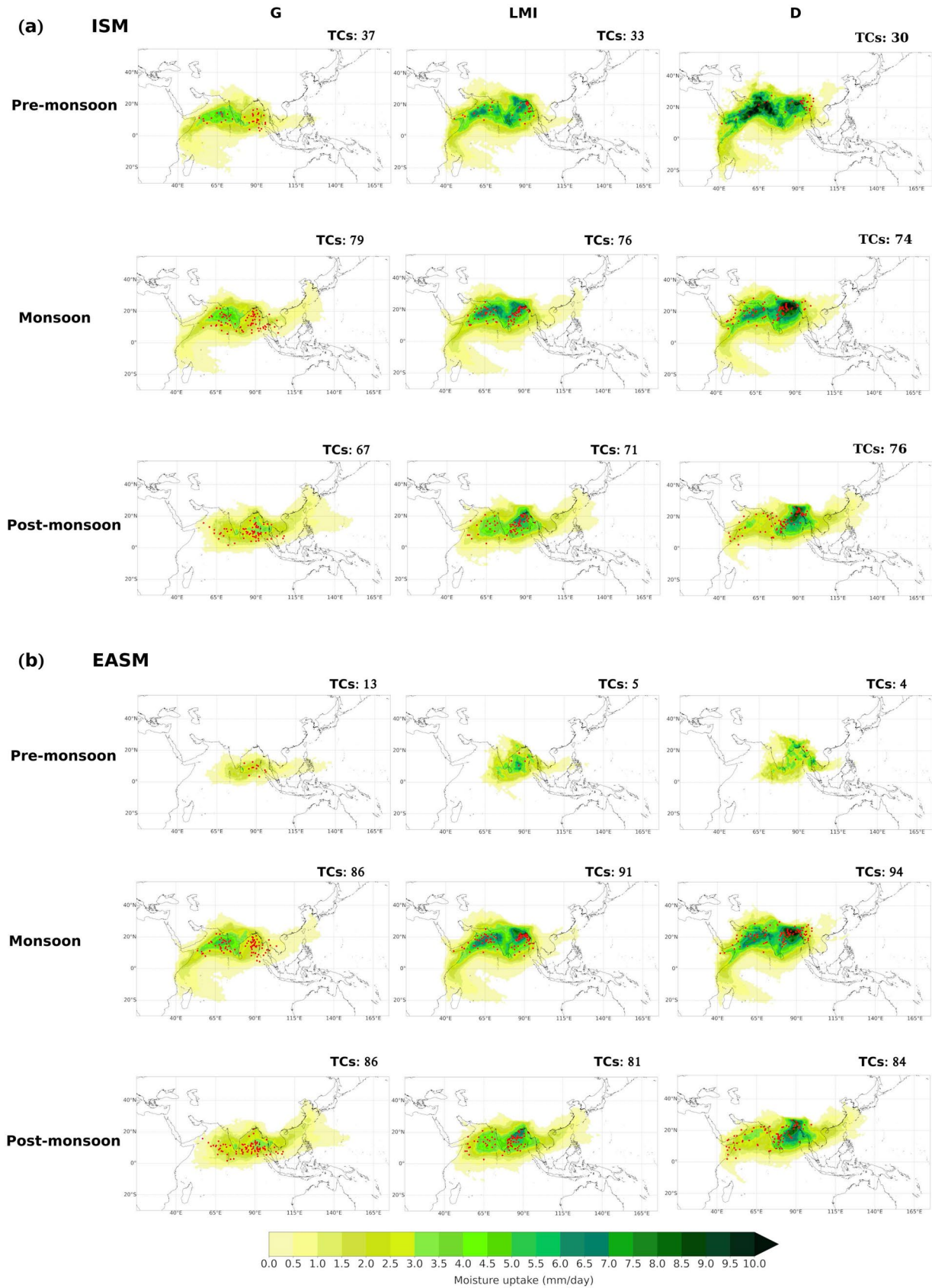


Fig. 14 Moisture uptake (greenish colour) for tropical cyclones (TCs) genesis, peak of maximum intensity, and dissipation over the NIO basin during the pre-monsoon, monsoon, and post-monsoon seasons for the **a** Indian Summer Monsoon (ISM) and **b** East Asian Summer Monsoon (EASM). Capital letters at the top indicate the TCs phases, genesis (G), lifetime maximum intensity (LMI), and dissipation (D). Red points indicate the TCs position in each stage. In the top right of each map is the number of TCs during each monsoon phase

the Arabian Sea accounted for 25.4% (D-N2, yellow), and the remaining 32.9% disappeared over the eastern coast of India and Bangladesh (D-N3, green). The SIO basin shows a cluster pattern for TC dissipation, similar to those for the genesis and LMI phases, although in this terminal phase, the TC positions within each cluster were more dispersed. One cluster was located in the central IO (D-S1, purple, 33.7%); one over the western coast of Australia (D-S2, cyan, 26%); and the third, which accounted for a higher number of TCs, appeared in the western IO (D-S3, orange, 40.1%).

The TC monthly distribution of each cluster revealed a high frequency of events from October to December in the NIO (Fig. 10b) and from December to April in the SIO (Fig. 10c). In both basins, the monthly distribution for TC dissipation showed a similar pattern to that observed for the prior life phases.

Over the NIO, the wind flux linked to the SLLJ appeared as the main mechanism of moisture transport from the western SIO and the eastern coast of Africa towards the D-N1 and D-N2 clusters, and the moisture uptake and VIMF patterns were more intense for D-N2 (Fig. 11a,b), supplying approximately 40–60% of moisture. For D-N1, the BoB and IP were the main moisture sources, supplying ~60–70% of moisture (Fig. 11d). Additionally, the moisture transported from the SCS was approximately 10% for D-N3 and D-N1. Furthermore, the inland GB exhibited the highest moisture supply (~65%) for D-N3 (Fig. 11c, f). According to Ying et al. (2005), the moisture supplied and the properties of the underlying surface have a significant effect on the TC rainfall distribution. Therefore, our results suggest that the moisture supplied is not only helpful in sustaining the TCs remnants at the dissipation stage over land but is also an essential condition for causing torrential rain.

In the SIO basin, the easterly winds linked to the northern branch of the MHPS transported much of the atmospheric moisture from the western coast of Australia and the Wharton Basin to D-S1 (Fig. 12a), contributing approximately 40–70% (Fig. 12b). For the D-S2 cluster, the Perth Basin, the north Australian basin, and the northwestern portion of mainland Australia supplied moisture in a range of ~45–70%, and the Australian monsoonal westerly winds transported the remaining amount (~5–20%) from the eastern IO (Fig. 12b,e). For D-S3, the central SIO through the easterly winds was the principal source (~40–65%), which

also received moisture from the eastern coast of Africa and the Somali basin (~20–35%), in Figs. 12c and f.

Similar to the TC genesis and LMI, Fig. 13 summarises the moisture sources and their contributions to the precipitation during the TC dissipation stage over the NIO and SIO basins. Figure 13a shows that the BoB, AS, GB, and IP were the main moisture sources in the NIO basin, providing ~60–80% (Fig. 13b). Additionally, the InP and the SCS along the coast of South China supplied ~20–30%, and the WIO provided the remaining ~10%. Similarly, from Fig. 13c, the WB, PB, and CIO were identified as the main sources of atmospheric humidity for the precipitation of TCs during the dissipation process in the SIO basin, supplying ~50–70% of moisture (Fig. 13d). Additionally, the moisture transported from the WIO was ~25–35% of the total amount, and the northwestern portion of Australia (NA) contributed ~5–10%. Overall, the oceanic (terrestrial) sources supplied ~81.83% (~18.17%) and ~83.17% (~16.82%) of moisture in NIO and SIO basins, respectively.

Regarding the MWVRT, no noticeable differences were found to the genesis and LMI stages. The MWVRT during the dissipation stage that formed over the NIO basin varied from 2.4 ± 0.5 (in D-N2) to 2.8 ± 0.5 (in D-N3) days; for the SIO basin, it was higher than for NIO, ranging from 2.7 ± 0.4 (in D-S2) to 3.1 ± 0.4 (in D-S1) days.

3.4 Relationship between monsoon systems and moisture sources

The region of the NIO basin is affected by the most important monsoon system, the Asian summer monsoon, which includes the Indian summer monsoon (ISM) and the East Asian Summer monsoon (EASM). The Asian summer monsoon ASM is considered a large-scale coupled ocean–atmosphere phenomenon and is associated with changes in atmospheric circulation patterns (Liu et al. 2019) over the region. Our findings revealed that on average, the ISM started on 01 June and ended on 26 October, the mean onset of EASM occurred on 02 May, and the offset was approximately on 16 October, in agreement with Noska and Misra (2016). Accordingly, 39.3% (42.8%) and 33.3% (42.8%) of TC genesis in the NIO occurred during the ISM (EASM) monsoon and post-monsoon seasons.

We also investigated the changes in the intensity and position of moisture sources for TCs over the NIO basin because of the different monsoon seasons (pre-monsoon, monsoon, and post-monsoon), as shown in Fig. 14 for the genesis, LMI, and dissipation phases, and in Figure S1 for the TS, H, and MH intensity categories. During the ISM pre-monsoon and monsoon seasons, the highest moisture contribution to TCs over the NIO basin was from the IP, AS, and WIO along the eastern coast of Africa. The moisture was mainly transported to the TC position by a strong

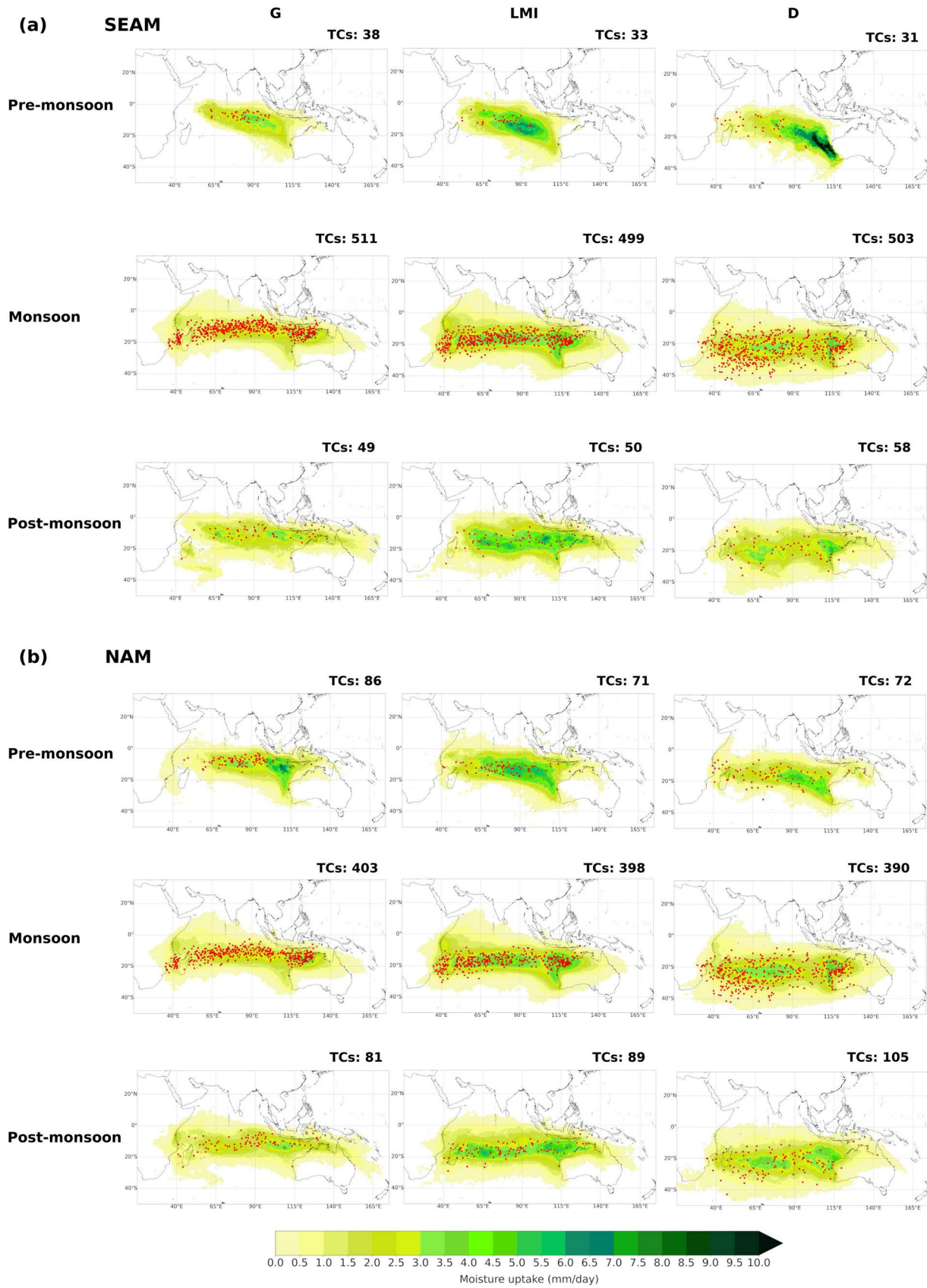


Fig. 15 Moisture uptake (greenish colour) for tropical cyclones (TCS) genesis, peak of maximum intensity and dissipation over the SIO basin during the pre-monsoon, monsoon and post-monsoon seasons for the **a** Southeastern African Monsoon (SEAM) and **b** North Australia Monsoon (NAM). Capital letters at the top indicate the TCs phases, genesis (G), lifetime maximum intensity (LMI), and dissipation (D). Red points indicate the TCs position in each stage. In the top right of each map is the number of TCs during each monsoon phase

cross-equatorial low-level jet stream (Joseph et al. 2006). Moreover, because the zonal branch of the Somali Jet forms during the boreal summer, moisture is advected eastward towards the ISM (Liebmann et al. 2012). That is, the ISM is associated with an increase in the precipitation, building up of vertically integrated humidity, strengthening of the low-level westerly wind over southwestern India and an increase in the kinetic energy (Krishnamurti 1985; Sahana et al. 2015). During the EASM pre-monsoon, the moisture gained by TCs was mainly from the southeastern AS, the IP, and the northern BoB. In general, a weak moisture contribution was observed from the BoB and the SCS. Nevertheless, during the post-monsoon season, the moisture uptake from the BoB and SCS was strengthened, and the moisture supplied from the AS and the Somali basin was lower than that of the pre-monsoon and monsoon seasons, being practically zero for TC genesis during the ISM pre-monsoon season. During all monsoon phases, the moisture sources supplied more moisture as the TCs became more intense, although the moisture gained by TCs during the dissipation phase was notably high.

The SIO basin is affected by the Southeastern African Monsoon (SEAM) and the North Australia Monsoon (NAM) occurring on both sides of the basin, in southeast Africa and the north Australia, respectively. According to our estimations, the SEAM started on approximately 08 November and ended on 16 April (as found by Kniveton et al. (2009), Shongwe et al. (2015) and Dunning et al. (2016)), and the NAM started on 13 December and ended on 25 March (in agreement with Suppiah (1992) and Pope et al. (2009)). Thus, 83.8% and 66.1% of the TCs generated in the SIO basin occurred during the SEAM and NAM monsoon seasons, respectively.

Figure 15 shows the intensity and position of moisture sources during the monsoon seasons for TC genesis, LMI, and dissipation phases over the SIO. Likewise, Figure S2 is similar to Fig. 15 but for the TS, H, and MH intensity categories. During the pre-monsoon period, the moisture supplied from the WB and PB was a more intense source during the NAM than during the SEAM and remained active throughout the TC season. During the SEAM and NAM monsoon seasons, the moisture contribution from the WIO and the northeastern coast of Africa was notable. The ISM reversal seasonal circulation (Funk et al. 2016) affects the moisture transport patterns in the region. Thus,

the southward movement of the continental tropical convergence zone and the subtropical anticyclone led to the winds blowing from the Indian subcontinent towards the IO in a northeasterly direction during the boreal winter, triggering the northeastern monsoon (Rajeevan et al. 2012), transporting moisture from the Arabian Sea along the east coast of Africa to the position of the TCs over the western basin of the SIO. In addition, during the post-monsoon season, the North Australia and the Coral Sea also contributed to atmospheric moisture for the precipitation associated with TC activity. In summary, TCs uptake more moisture during intensity changes than during the genesis or dissipation phases (Figs. 15 and S2).

Overall, the largest differences in the moisture uptake pattern during the monsoon phases (pre-monsoon, monsoon and post-monsoon) occurred over the NIO basin. This behaviour is probably caused by the intensity of the ISM and EASM compared to the SEAM and NAM. Note that the intensity of the former is notably higher than the latter (Liu et al. 2019). It is worth noting that experiments (e.g. Clemens and Prell 2003) with atmospheric global circulation models have revealed that the elevation of Himalaya-Tibet has significant effects on the intensity of the Asia Summer Monsoon.

Furthermore, according to Table 2, in general, the largest Lagrangian MWVRT observed in the NIO was during the post-monsoon season, and for the SIO basin, during the pre-monsoon season. Regardless of the monsoon season, in both basins, TCs exhibited the highest MWVRT during the genesis phase and the lowest during the dissipation stage, always having in all cases, as discussed, higher values in the SIO than in the NIO basin.

4 Conclusion and remarks

Tropical cyclones (TCs) are one of the most destructive weather phenomena that affect coastal countries in tropical regions, producing major impacts over significantly large areas. In this study, a Lagrangian approach was used to identify the origin of TC precipitation during the genesis, intensification, and dissipation stages over the Indian Ocean. We objectively separated the locations of TC genesis, lifetime maximum intensification, and dissipation stages into clusters in both the North Indian Ocean (NIO) and the South Indian Ocean (SIO) basins to determine the moisture sources and moisture transport mechanisms in these regions. The position and size of each TC formed in the NIO and SIO from 1980 to 2018 were extracted from the Joint Typhoon Warning Centre best track archives and the TCSize database, respectively.

A Lagrangian moisture source diagnostic method was applied to the backward trajectories of atmospheric parcels

Table 2 Lagrangian mean water vapour residence time (in days) during monsoon seasons for the TCs genesis (G), lifetime maximum intensity (LMI) intensity changes, and dissipation (D) in the North Indian Ocean (NIO) and South Indian Ocean (SIO) basins

Basin	G	LMI	TS	H	MH	D
NIO						
ISM						
Pre-	3.0±0.3	2.6±0.4	2.9±0.3	2.7±0.3	2.6±0.3	2.5±0.3
Mon	3.0±0.4	2.5±0.4	2.8±0.4	2.7±0.3	2.8±0.3	2.5±0.4
Post-	3.3±0.6	2.9±0.7	3.1±0.7	3.0±0.6	2.7±0.4	2.8±0.5
EASM						
Pre-	3.1±0.6	2.6±0.5	2.9±0.4	2.8±0.4	2.9±0.1	2.3±0.6
Mon	3.0±0.3	2.6±0.3	2.8±0.4	2.7±0.3	2.5±0.3	2.5±0.3
Post-	3.3±0.6	2.8±0.5	3.1±0.5	2.9±0.5	2.8±0.4	2.7±0.6
SIO						
SEAM						
Pre-	3.5±0.4	3.2±0.3	3.3±0.4	3.3±0.3	3.7±0.1	3.2±0.4
Mon	3.3±0.5	3.1±0.4	3.2±0.4	3.1±0.4	3.2±0.4	2.9±0.4
Post-	3.2±0.3	3.1±0.4	3.1±0.4	3.0±0.3	3.0±0.3	2.8±0.3
NAM						
Pre-	3.4±0.7	3.3±0.6	3.3±0.6	3.2±0.6	3.4±0.4	3.0±0.6
Mon	3.2±0.4	3.1±0.4	3.2±0.4	3.1±0.4	3.1±0.5	2.9±0.4
Post-	3.3±0.4	3.1±0.4	3.2±0.4	3.0±0.4	3.0±0.4	2.9±0.3

TS: Tropical Storm, H: Hurricanes (category 1 and 2 on the Saffir-Simpson scale) and MH: Major Hurricane (category 3+ on Saffir-Simpson scale). Pre-, Mon and Post- referred to Pre-monsoon, Monsoon and Post-monsoon seasons, respectively

ISM: Indian Summer Monsoon, EASM: East Asian Summer Monsoon, SEAM: Southeastern African Monsoon, NAM: North Australia Monsoon

residing over the area occupied by the TC outer radius to identify the moisture sources. The pathways of the parcels were obtained from the global outputs of the Lagrangian model FLEXPART, forced with the ERA-Interim reanalysis data.

This study revealed that in the NIO basin, the Bay of Bengal, the Arabian and South China Sea were the predominant oceanic moisture sources for TC activity, and continental areas such as the Indian Peninsula, the Ganges basin and the southern coast of China also contributed to the moisture supply for the genesis, intensification, and dissipation stages. We also found that the western Indian Ocean and the eastern coast of Africa were a notable moisture sources through the SLLJ for TCs that occurred over the Arabian Sea. Notably, for the TCs over the Bay of Bengal the most intense source of moisture was the Ganges River basin when the TCs were at their most intense phase.

For the cyclogenesis and development of TCs over the SIO basin, the central Indian Ocean, the Wharton and the Perth basins were identified as the main moisture sources that supply the precipitant atmospheric humidity throughout the easterly trade winds blowing out the Mascarene High pressure system. Moreover, the Western Indian Ocean, the northern Australian mainland, and the Coral Sea contributed to the moisture supply but with less intensity. The climatological pattern of moisture uptake revealed that during the intensification process, TCs

gained more moisture for precipitation than during the genesis and dissipation stages. Overall, the differences found in the moisture uptake pattern during the different phases of TCs development over the Indian Ocean were statistically significant at a 95% significance level. In summary, the oceanic (terrestrial) sources supplied ~86% (~14%) of moisture in the NIO basin and ~80% (~20%) in the SIO basin.

In both basins, TCs required more atmospheric humidity during intensity changes to hurricanes than to major hurricanes or tropical storms. This finding was also supported by computing the average of total specific humidity in the atmospheric column enclosed by the TC outer radius. Figure S3 reveals that the mean total specific humidity increased in both basins from genesis, reaching its maximum value for the hurricane category and then decreasing for the dissipation stage. Additionally, we compared the moisture uptake pattern of each TC phase with respect to the genesis phase by applying the statistical t-Student test. Furthermore, the moisture sources that supply atmospheric humidity for TC activity over the NIO basin were more heavily modulated by monsoon systems than those over the SIO.

The Lagrangian methodology used in this work allowed us to find that the time taken by the moisture for precipitation to reach the TCs differs for both basins, being faster for the NIO (from 2.6 to 3.1 days) than for the SIO (from 2.9 to 3.2 days). Overall, the highest time was during the

genesis phase and tropical storm intensity category, and the lowest was during the dissipation stage. Differences were also found in monsoonal episodes. On average, these times were higher during the post-monsoon season in the NIO and during the pre-monsoon season in the SIO. In general, the time values it takes for precipitant moisture to reach the TCs are lower than the climatological estimations by Läderach and Sodemann (2016) and Sodemann (2020) for the global tropics (4.5 to 5.8 days) for which they did not differentiate weather systems, including in their estimates for all days of the year and any weather situation, unlike our work.

Climate and meteorological dynamics are influenced by modes of climate variability, such as the Indian Ocean Dipole and El Niño-Southern Oscillation. They modulate TC activity and can also affect the moisture transport for the TCs. In further research, it will be necessary to focus our attention on the role of these modes in the variability of the intensity and extent of moisture sources for precipitation originating from TCs during their lifetime. In addition, the findings from this study will also be used as a reference in future works to identify changes in the intensity and position of moisture sources for precipitation associated with TCs over the Indian Ocean in the different climate scenarios projections.

Supplementary Information The online version contains supplementary material available at <https://doi.org/10.1007/s00382-022-06429-4>.

Acknowledgements A.P-A acknowledges a PhD grant from the University of Vigo. J.C.F-A and R.S thanks the Xunta de Galicia (Galician Regional Government) for support this study under the grants no. ED481A-2020/193 and ED481B 2019/070, respectively. The authors thanks to JTWC for the best track archive database and to Copernicus Climate Change Service for the ERA-Interim reanalysis. We acknowledge the partial support from the Xunta de Galicia under the Project ED431C 2021/44. This work has been also possible thanks to the computing resources and technical support provided by CESGA (Centro de Supercomputacion de Galicia). We acknowledge the funding for open access from the Universidade de Vigo/Consortio Interuniversitario do Sistema Universitario de Galicia.

Author contributions Conceptualization: LG, RN, AP-A; Methodology: LG, RN, APA, RS; Formal analysis and investigation: AP-A, JCF-A, RS; Writing—original draft preparation: AP-A; Writing—review and editing: AP-A; RS, RN, LG, JCF-A; Supervision: LG, RN. All authors read and approved the final manuscript.

Funding Open Access funding provided thanks to the CRUE-CSIC agreement with Springer Nature. This research is supported by the LAGRIMA and SETESTRELO projects (grants no. RTI2018-095772-B-I00 and PID2021-122314OB-I00, respectively) funded by the Ministerio de Ciencia, Innovación y Universidades, Spain. Partial support was also obtained from the Xunta de Galicia, Consellería de Cultura, Educación e Universidade, under project ED431C 2021/44 “Programa de Consolidación e Estructuración de Unidades de Investigación Competitivas”.

Data availability The datasets used during the current study are available online. The best track archive database from the JTWC is

accessible at <https://www.metoc.navy.mil/jtwc/jtwc.html?best-tracks> and the the ERA-Interim reanalysis at <https://apps.ecmwf.int/datasets/data/interim-full-daily/levtype=sfc>. The Multi-Source Weighted-Ensemble Precipitation (MSWEP) v2 was obtained from <http://www.gloh2o.org/mswep/>, and the TCSIZE database was from <http://doi.org/10.17632/8997r89fbf.1>. The FLEXPART model source code is available at <https://www.flexpart.eu/downloads/6>.

Declarations

Conflict of interest The authors declare no conflict of interest.

Open Access This article is licensed under a Creative Commons Attribution 4.0 International License, which permits use, sharing, adaptation, distribution and reproduction in any medium or format, as long as you give appropriate credit to the original author(s) and the source, provide a link to the Creative Commons licence, and indicate if changes were made. The images or other third party material in this article are included in the article's Creative Commons licence, unless indicated otherwise in a credit line to the material. If material is not included in the article's Creative Commons licence and your intended use is not permitted by statutory regulation or exceeds the permitted use, you will need to obtain permission directly from the copyright holder. To view a copy of this licence, visit <http://creativecommons.org/licenses/by/4.0/>.

References

- Aemisegger F, Papritz L (2018) A climatology of strong large-scale ocean evaporation events. Part I: Identification, global distribution, and associated climate conditions. *J Clim* 31(18):7287–7312. <https://doi.org/10.1175/JCLI-D-17-0591.1>
- Barimalala R, Desbiolles F, Blamey RC, Reason C (2018) Madagascar influence on the South Indian Ocean Convergence Zone, the Mozambique Channel Trough and southern African rainfall. *Geophys Res Lett* 45(11):380–389. <https://doi.org/10.1029/2018GL079964>
- Beck HE, Wood EF, Pan M, Fisher CK, Miralles DG, van Dijk AIJM, McVicar TR, Adler RF (2019) MSWEP V2 Global 3–Hourly 0.1° Precipitation: Methodology and Quantitative Assessment. *Bull Am Meteorol Soc* 100:473–500. <https://doi.org/10.1175/BAMS-D-17-0138.1>
- Bhatla R, Raj R, Mall RK, Shivani (2020) Tropical Cyclones over the North Indian Ocean in changing climate. In: Srivastava PK, Singh SK, Mohanty UC, Murty T (eds) Techniques for disaster risk management and mitigation. Wiley Online Library, New Jersey. <https://doi.org/10.1002/9781119359203.ch5>
- Boruff BJ (2009) Environmental hazards: assessing risk and reducing disasters, 5th edition by Keith Smith and David N. Petley. *Geogr Res* 47:454–455. <https://doi.org/10.1111/j.1745-5871.2009.00611.x>
- Bousquet O, Barruol G, Cordier E, Barthe C, Bielli S, Calmer R, Rindharisaona E, Roberts G, Tulet P, Amelie V, et al. (2021) Impact of tropical cyclones on inhabited areas of the swio basin at present and future horizons. part 1: overview and observing component of the research project RENOVRIK-CYCLONE. *Atmosphere* 12:544. <https://doi.org/10.3390/atmos12050544>
- Brioude J, Arnold D, Stohl A, Cassiani M, Morton D, Seibert P, Angevine W, Evan S, Dingwell A, Fast JD, Easter RC, Pissio I, Burkhardt J, Wotawa G (2013) The Lagrangian particle dispersion

- model FLEXPART-WRF version 3.1. *Geosci Model Dev* 6:1889–1904. <https://doi.org/10.5194/gmd-6-1889-2013>
- Clemens SC, Prell WL (2003) A 350,000 year summer-monsoon multiproxy stack from the Owen Ridge, Northern Arabian Sea. *Mar Geol* 201(1–3):35–51. [https://doi.org/10.1016/S0025-3227\(03\)00207-X](https://doi.org/10.1016/S0025-3227(03)00207-X)
- Corporal-Lodangco I-L, Richman MB, Leslie LM, Lamb PJ (2014) Cluster analysis of north atlantic tropical cyclones. *Proced Comput Sci* 36:293–300. <https://doi.org/10.1016/j.procs.2014.09.096>
- Dee DP et al (2011) The ERA-Interim reanalysis: configuration and performance of the data assimilation system. *Q J R Meteorol* 137:553–597. <https://doi.org/10.1002/qj.828>
- DeMott CA, Klingaman NP, Woolnough SJ (2015) Atmosphere-ocean coupled processes in the Madden-Julian oscillation. *Rev Geophys* 53:1099–1154. <https://doi.org/10.1002/2014RG000478>
- Dominguez C, Magaña V (2018) The role of tropical cyclones in precipitation over the tropical and subtropical North America. *Front Earth Sci* 6:19. <https://doi.org/10.3389/feart.2018.00019>
- Drosowsky W (1996) Variability of the Australian summer monsoon at Darwin: 1957–1992. *J Clim* 9(1):85–96. [https://doi.org/10.1175/1520-0442\(1996\)09<0092:CO;2](https://doi.org/10.1175/1520-0442(1996)09<0092:CO;2)
- Dunning CM, Black ECL, Allan RP (2016) The onset and cessation of seasonal rainfall over Africa. *J Geophys Res Atmos* 121:405–424. <https://doi.org/10.1002/2016JD025428>
- Emanuel K, De Autels C, Holloway C, Korty R (2004) Environmental control of tropical cyclone intensity. *J Atmos Sci* 61:843–858. [https://doi.org/10.1175/1520-0469\(2004\)061%3c0843:ECOTCI%3e2.0.CO;2](https://doi.org/10.1175/1520-0469(2004)061%3c0843:ECOTCI%3e2.0.CO;2)
- Funk C, Hoell A, Shukla S, Husak G, Michaelsen J (2016) The east African monsoon system: seasonal climatologies and recent variations. In: de Carvalho L, Jones C (eds) *The monsoons and climate change*, Springer Climate. Springer, Cham. https://doi.org/10.1007/978-3-319-21650-8_8
- Gimeno L, Drumond A, Nieto R, Trigo RM, Stohl A (2010) On the origin of continental precipitation. *Geophys Res Lett* 37:L13804. <https://doi.org/10.1029/2010GL043712>
- Gimeno L, Stohl A, Trigo RM, Dominguez F, Yoshimura K, Yu L, Drumond A, Durán-Quesada AM, Nieto R (2012) Oceanic and terrestrial sources of continental precipitation. *Rev Geophys* 50:RG4003. <https://doi.org/10.1029/2012RG000389>
- Gimeno L, Vázquez M, Eiras-Barca J, Sorí R, Stojanovic M, Algarra I, Nieto R, Ramos AM, Durán-Quesada AM, Dominguez F (2020) Recent progress on the sources of continental precipitation as revealed by moisture transport analysis. *Earth-Sci Rev* 201:103070. <https://doi.org/10.1016/j.earscirev.2019.103070>
- Gimeno L, Eiras-Barca J, Durán-Quesada AM, Dominguez F, van der Ent R, Sodemann H, Sánchez-Murillo R, Nieto R, Kirchner JW (2021) The residence time of water vapour in the atmosphere. *Nat Rev Earth Environ* 2(8):558–569. <https://doi.org/10.1038/s43017-021-00181-9>
- Gray WM (1968) Global view of the origin of tropical disturbances and storms. *Mon Weather Rev* 96:669–700. [https://doi.org/10.1175/1520-0493\(1968\)096%3c0669:GVOTOO%3e2.0.CO;2](https://doi.org/10.1175/1520-0493(1968)096%3c0669:GVOTOO%3e2.0.CO;2)
- Gray WM (1977) Tropical cyclone genesis in the Western North Pacific. *J Meteorol Soc Jpn Ser II* 55:465–482. https://doi.org/10.2151/jmsj1965.55.5_465
- Halpern D, Woiceshyn PM (1999) Onset of the Somali Jet in the Arabian Sea during June 1997. *J Geophys Res* 104:18041–18046. <https://doi.org/10.1029/1999JC900141>
- Hartigan J, Wong M (1979) Algorithm AS 136: a K-means clustering algorithm. *J R Stat Soc Ser C Appl Stat* 28(1):100–108. <https://doi.org/10.2307/2346830>
- Henderson-Sellers A, McGuffie K, Zhang H (2002) Stable isotopes as validation tools for global climate model predictions of the impact of Amazonian deforestation. *J Clim* 15:2664–2677. [https://doi.org/10.1175/1520-0442\(2002\)015%3c2664:SIA-VTF%3e2.0.CO;2](https://doi.org/10.1175/1520-0442(2002)015%3c2664:SIA-VTF%3e2.0.CO;2)
- Hermes JC, Masumoto Y, Beal LM, Roxy MK, Vialard J, Andres M, Annamalai H et al (2019) A sustained ocean observing system in the Indian Ocean for climate related scientific knowledge and societal needs. *Front Mar Sci* 6:355. <https://doi.org/10.3389/fmars.2019.00355>
- Hersbach H, Bell B, Berrisford P, Hirahara S, Horányi A, Muñoz-Sabater J, Nicolas J, Peubey C et al (2020) The ERA5 global reanalysis. *Q J R Meteorol Soc* 146:1999–2049. <https://doi.org/10.1002/qj.3803>
- Joseph PV, Sooraj KP, Rajan CK (2006) The summer monsoon onset process over South Asia and an objective method for the date of monsoon onset over Kerala. *Int J Climatol* 26:1871–1893. <https://doi.org/10.1002/joc.1340>
- Kaufman L, Rousseeuw PJ (2005) *Finding groups in data: an introduction to cluster analysis*. Wiley Series in Probability and Statistics, New Jersey
- Kiguchi M, Matsumoto J (2005) The rainfall phenomena during the pre-monsoon period over the Indochina Peninsula in the GAME-IOP Year, 1998. *J Meteorol Soc Japan* 83(1):89–106. <https://doi.org/10.2151/jmsj.83.89>
- Kniveton DR, Layberry R, Williams CJR, Peck M (2009) Trends in the start of the wet season over Africa. *Int J Climatol* 29(9):1216–1225. <https://doi.org/10.1002/joc.1792>
- Krishnamurti TN (1985) Summer monsoon experiment: a review. *Mon Weather Rev* 113:1590–1626. [https://doi.org/10.1175/1520-0493\(1985\)113%3c1590:SMER%3e2.0.CO;2](https://doi.org/10.1175/1520-0493(1985)113%3c1590:SMER%3e2.0.CO;2)
- Läderach A, Sodemann H (2016) A revised picture of the atmospheric moisture residence time. *Geophys Res Lett* 43:924–933. <https://doi.org/10.1002/2015GL067449>
- Lazenby MJ, Todd MC, Wang Y (2016) Climate model simulation of the South Indian Ocean Convergence zone: mean state and variability. *Clim Res* 68(1):59–71. <https://doi.org/10.3354/cr01382>
- Li Z, Yu W, Li T, Murty VSN, Tangang F (2013) Bimodal character of cyclone climatology in the bay of Bengal modulated by monsoon seasonal cycle. *J Clim* 26:1033–1046. <https://doi.org/10.1175/JCLI-D-11-00627.1>
- Liebmann B, Bladé I, Kiladis GN, Carvalho LMV, Senay GB, Allured D, Leroux S, Funk C (2012) Seasonality of African precipitation from 1996 to 2009. *J Clim* 25(12):4304–4322. <https://doi.org/10.1175/JCLI-D-11-00157.1>
- Lisonbee J, Ribbe J, Wheeler M (2020) Defining the north Australian monsoon onset: a systematic review. *Prog Phys Geogr* 44(3):398–418. <https://doi.org/10.1177/0309133319881107>
- Liu Y, Liang P, Sun Y (2019) Basic features of the Asian summer monsoon system. *The Asian summer monsoon: characteristics, variability, teleconnections and projection*. Elsevier, Amsterdam, p 237
- Longshore D (2009) *Encyclopedia of Hurricanes, Typhoons, and Cyclones*, Infobase Publishing, New York, p 467
- MacQueen J (1967) Some methods for classification and analysis of multivariate observations. *Proceedings of fifth Berkeley symposium on mathematical statistics and probability*. University of California, Berkeley, pp 281–297
- Manatsa D, Morioka Y, Behera SK, Matarira CH, Yamagata T (2014) Impact of Mascarene High variability on the East African ‘short rains’. *Clim Dyn* 42:1259–1274. <https://doi.org/10.1007/s00382-013-1848-z>
- Martínez JA, Dominguez F (2014) Sources of atmospheric moisture for the La Plata River basin. *J Clim* 27:6737–6753. <https://doi.org/10.1175/JCLI-D-14-00022.1>
- Mohapatra M, Bandyopadhyay BK, Tyagi A (2012) Best track parameters of tropical cyclones over the North Indian Ocean: a review. *Nat Hazards* 63:1285–1317. <https://doi.org/10.1007/s11069-011-9935-0>

- Muni KK (2009) Intensifying tropical cyclones over the North Indian Ocean during summer monsoon-global warming. *Glob Planet Change* 65(1–2):12–16. <https://doi.org/10.1016/j.gloplacha.2008.10.007>
- Nakamura J, Lall U, Kushnir Y, Camargo SJ (2009) Classifying North Atlantic tropical cyclone tracks by mass moments. *J Clim* 22:5481–5494. <https://doi.org/10.1175/2009JCLI2828.1>
- Needham HF, Keim BD, Sathiaraj D (2015) A review of tropical cyclone-generated storm surges: global data sources, observations, and impacts. *Rev Geophys* 53:545–591. <https://doi.org/10.1002/2014RG000477>
- Nieto R, Castillo R, Drumond A (2014) The modulation of oceanic moisture transport by the hemispheric annular modes. *Front Earth Sci* 2:11. <https://doi.org/10.3389/feart.2014.00011>
- Ninomiya K (2008) Similarities and differences among the South Indian Ocean Convergence Zone, North American convergence zone, and other subtropical convergence zones simulated using an AGCM. *J Meteorol Soc Jpn Ser II* 86(1):141–165. <https://doi.org/10.2151/jmsj.86.141>
- Noska R, Misra V (2016) Characterizing the onset and demise of the Indian summer monsoon. *Geophys Res Lett* 43:4547–4554. <https://doi.org/10.1002/2016GL068409>
- Numaguti A (1999) Origin and recycling processes of precipitating water over the Eurasian continent: Experiments using an atmospheric general circulation model. *J Geophys Res* 104:1957–1972. <https://doi.org/10.1029/1998JD20002>
- Ordoñez P, Ribera P, Gallego D, Peña-Ortiz C (2012) Major moisture sources for Western and Southern India and their role on synoptic-scale rainfall events. *Hydrol Process* 26:3886–3895. <https://doi.org/10.1002/hyp.8455>
- Pazos M, Gimeno L (2017) Identification of moisture sources in the Atlantic Ocean for cyclogenesis processes. In: Proceedings of the 1st International Electronic Conference on Hydrological Cycle (ChyCle-2017). Sciforum Electronic Conf Ser. <https://doi.org/10.3390/CHyCle-2017-04862>
- Pérez-Alarcón A, Sorí R, Fernández-Alvarez JC, Nieto R, Gimeno L (2021) Comparative climatology of outer tropical cyclone size using radial wind profiles. *Weather Clim Extrem* 33:100366. <https://doi.org/10.1016/j.wace.2021.100366>
- Pérez-Alarcón A, Sorí R, Fernández-Alvarez JC, Nieto R, Gimeno L (2022a) Where does the moisture for North Atlantic tropical cyclones come from? *J Hydrometeorol*. <https://doi.org/10.1175/JHM-D-21-0117.1>
- Pérez-Alarcón A, Coll-Hidalgo P, Fernández-Alvarez JC, Sorí R, Nieto R, Gimeno L (2022b) Moisture sources for precipitation associated with major hurricanes during 2017 in the North Atlantic basin. *J Geophys Res Atmos* 127:e2021JD035554. <https://doi.org/10.1029/2021JD035554>
- Pérez-Alarcón A, Sorí R, Fernández-Alvarez JC, Nieto R, Gimeno L (2022c) Dataset of outer tropical cyclone size from a radial wind profile. *Data BR* 40:107825. <https://doi.org/10.1016/j.dib.2022.107825>
- Pope M, Jakob C, Reeder MJ (2009) Regimes of the north Australian wet season. *J Clim* 22:6699–6715. <https://doi.org/10.1175/2009JCLI3057.1>
- Rahman M, Yang R, Di L (2018) Clustering Indian ocean tropical cyclone tracks by the standard deviational ellipse. *Climate* 6(2):39. <https://doi.org/10.3390/cli6020039>
- Rajeevan M, Unnikrishnan CK, Bhate J, Niranjana-Kumar K, Sreekala PP (2012) Northeast monsoon over India: variability and prediction. *Meteorol Appl* 19:226–236. <https://doi.org/10.1002/met.1322>
- Rousseeuw PJ (1987) Silhouettes: a graphical aid to the interpretation and validation of cluster analysis. *J Comput Appl Math* 20:53–65. [https://doi.org/10.1016/0377-0427\(87\)90125-7](https://doi.org/10.1016/0377-0427(87)90125-7)
- Sahana AS, Ghosh S, Ganguly A, Murtugudde R (2015) Shift in Indian summer monsoon onset during 1976/1977. *Environ Res Lett* 10(5):054006. <https://doi.org/10.1088/1748-9326/10/5/054006>
- Samson G, Masson S, Lengaigne M, Keerthi MG, Vialard J, Pous S, Madec G, Jourdain NC, Jullien S, Menkes C, Marchesiello P (2014) The NOW regional coupled model: application to the tropical Indian Ocean climate and tropical cyclone activity. *J Adv Model Earth Syst* 6:700–722. <https://doi.org/10.1002/2014M5000324>
- Shongwe ME, Lennard C, Liebmann B, Kalogomou EA, Ntsangwane L, Pinto I (2015) An evaluation of CORDEX regional climate models in simulating precipitation over southern Africa. *Atmos Sci Lett* 16(3):199–207. <https://doi.org/10.1002/asl2.538>
- Skamarock W, Klemp J, Dudhi J, Gill D, Barker D, Duda M, Huang X-Y, Wang W, Powers J (2008) A description of the advanced research WRF version 3. Tech Rep. <https://doi.org/10.5065/D6DZ069T>
- Sodemann H (2020) Beyond turnover time: constraining the lifetime distribution of water vapor from simple and complex approaches. *J Atmos Sci* 77(2):413–433. <https://doi.org/10.1175/JAS-D-18-0336.1>
- Sodemann H, Schwierz C, Wernli H (2008) Interannual variability of Greenland winter precipitation sources: Lagrangian moisture diagnostic and North Atlantic Oscillation influence. *J Geophys Res Atmos* 113:D03107. <https://doi.org/10.1029/2007JD008503>
- Sorí R, Nieto R, Drumond A, Vicente-Serrano SM, Gimeno L (2017) The atmospheric branch of the hydrological cycle over the Indus, Ganges, and Brahmaputra river basins. *Hydrol Earth Syst Sci* 21:6379–6399. <https://doi.org/10.5194/hess-21-6379-2017>
- Sprenger M, Wernli H (2015) The LAGRANTO Lagrangian analysis tool – version 2.0. *Geosci Model Dev* 8(8):2569–2586. <https://doi.org/10.5194/gmd-8-2569-2015>
- Stohl A, James PA (2004) Lagrangian analysis of the atmospheric branch of the global water cycle. Part I: method description, validation, and demonstration for the August 2002 flooding in Central Europe. *J Hydrometeorol* 5:656–678. [https://doi.org/10.1175/1525-7541\(2004\)005%3c0656:ALAOTA%3e2.0.CO;2](https://doi.org/10.1175/1525-7541(2004)005%3c0656:ALAOTA%3e2.0.CO;2)
- Stohl A, James PA (2005) A Lagrangian analysis of the atmospheric branch of the global water cycle: part II: earth's river catchments ocean basins, and moisture transports between them. *J Hydrometeorol* 6:961–984. <https://doi.org/10.1175/JHM470.1>
- Stohl A, Forster C, Frank A, Seibert P, Wotawa G (2005) Technical note: the Lagrangian particle dispersion model FLEXPART version 6.2. *Atmos Chem Phys* 5:2461–2474. <https://doi.org/10.5194/acp-5-2461-2005>
- Suppiah R (1992) The Australian summer monsoon: a review. *Prog Phys Geogr* 16(3):283–318. <https://doi.org/10.1177/030913339201600302>
- Tegtmeier S, Marandino C, Jia Y, Quack B, Mahajan AS (2022) Atmospheric gas-phase composition over the Indian Ocean. *Atmos Chem Phys* 22(10):6625–6676. <https://doi.org/10.5194/acp-22-6625-2022>
- Viswanadhapalli Y, Dasari HP, Dwivedi S, Madineni VR, Langodan S, Hoteit I (2020) Variability of monsoon low-level jet and associated rainfall over India. *Int J Climatol* 40:1067–1089. <https://doi.org/10.1002/joc.6256>
- van der Ent RJ, Tuinenburg OA (2017) The residence time of water in the atmosphere revisited. *Hydrol Earth Syst Sci* 21:779–790. <https://doi.org/10.5194/hess-21-779-2017>
- Van der Ent RJ, Wang-Erlandsson L, Keys PW, Savenije HHG (2014) Contrasting roles of interception and transpiration in the hydrological cycle—Part 2: moisture recycling. *Earth Syst Dyn* 5(2):471–489. <https://doi.org/10.5194/esd-5-471-2014>
- Wahiduzzaman M (2021) Major floods and tropical cyclones over Bangladesh: clustering from ENSO timescales. *Atmosphere* 12(6):692. <https://doi.org/10.3390/atmos12060692>

- Wang YP, Cui XP, Li XF, Zhang WL, Huang YJ (2016) Kinetic energy budget during the genesis period of tropical cyclone Dorian (2001) in the South China Sea. *Mon Weather Rev* 144:2831–2854. <https://doi.org/10.1175/MWR-D-15-0042.1>
- Williams GJ (2016) The inner core thermodynamics of the tropical cyclone boundary layer. *Meteorol Atmos Phys* 128:545–564. <https://doi.org/10.1007/s00703-016-0441-5>
- Wu L, Su H, Fovell RG, Dunkerton TJ, Wang Z, Kahn BH (2015) Impact of environmental moisture on tropical cyclone intensification. *Atmos Chem Phys* 15:14041–14053. <https://doi.org/10.5194/acp-15-14041-2015>
- Xu H, Zhai G, Li X (2017) Precipitation efficiency and water budget of Typhoon Fitow 787 (2013): a particle trajectory study. *J Hydrometeorol* 18(9):2331–2354. <https://doi.org/10.1175/JHM-D-16-0273.1>
- Xulu NG, Chikoore H, Bopape MJM, Nethengwe NS (2020). Climatology of the mascarene high and its influence on weather and climate over Southern Africa. *Climate* 8(7):86. <https://doi.org/10.3390/cli8070086>
- Yanase W, Satoh M, Taniguchi H, Fujinami H (2012) Seasonal and intraseasonal modulation of tropical cyclogenesis environment over the Bay of Bengal during the extended summer monsoon. *J Clim* 25:2914–2930. <https://doi.org/10.1175/JCLI-D-11-00208.1>
- Yuan J, Gao Y, Feng D, Yang Y (2019) The zonal dipole pattern of tropical cyclone genesis in the Indian Ocean influenced by the tropical Indo-Pacific Ocean sea surface temperature anomalies. *J Clim* 32(19):6533–6549. <https://doi.org/10.1175/JCLI-D-19-0042.1>

Publisher's Note Springer Nature remains neutral with regard to jurisdictional claims in published maps and institutional affiliations.